Title: The potassium channel subunit $K_V1.8$ (*Kcna10*) is essential for the distinctive outwardly rectifying conductances of type I and II vestibular hair cells

Hannah R. Martin[1], ORCID 0000-0003-2028-5798
Anna Lysakowski[2], ORCID 0000-0001-6259-0294
Ruth Anne Eatock[1], ORCID 0000-0001-7547-2051

[1]University of Chicago, Department of Neurobiology
[2]University of Illinois at Chicago, Department of Anatomy and Cell Biology

Author for correspondence:
Ruth Anne Eatock
Dept of Neurobiology, J251
University of Chicago
Chicago, IL
eatock@uchicago.edu

Keywords: potassium channels, hair cells, vestibular, inner ear, receptor potential

Abstract

In amniotes, head motions and tilt are detected by two types of vestibular hair cells (HCs) with strikingly different morphology and physiology. Mature type I HCs express a large and very unusual potassium conductance, $g_{K,L}$, which activates negative to resting potential, confers very negative resting potentials and low input resistances, and enhances an unusual non-quantal transmission from type I cells onto their calyceal afferent terminals. Following clues pointing to $K_V1.8$ (KCNA10) in the Shaker K channel family as a candidate $g_{K,L}$ subunit, we compared whole-cell voltage-dependent currents from utricular hair cells of $K_V1.8$-null mice and littermate controls. We found that $K_V1.8$ is necessary not just for $g_{K,L}$ but also for fast-inactivating and delayed rectifier currents in type II HCs, which activate positive to resting potential. The distinct properties of the three $K_V1.8$-dependent conductances may reflect different mixing with other K_V1 subunits, such as $K_V1.4$ (KCNA4). In $K_V1.8$-null HCs of both types, residual outwardly rectifying conductances include K_V7 (KCNQ) channels.

Current clamp records show that in both HC types, $K_V1.8$-dependent conductances increase the speed and damping of voltage responses. Features that speed up vestibular receptor potentials and non-quantal afferent transmission may have helped stabilize locomotion as tetrapods moved from water to land.

Graphical abstract

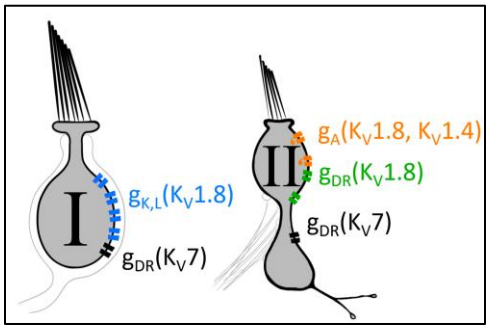

Abbreviations:

g_A, A-type (inactivating) K_V conductance in type II HCs

g_{DR}, delayed rectifier K^+ conductance

$g_{K,L}$, low-voltage-activated K^+ conductance in type I HCs

HC, hair cell

K_V, voltage-gated K^+ conductance

Introduction

The receptor potentials of hair cells (HCs) are strongly shaped by large outwardly rectifying K^+ conductances that are differentially expressed according to HC type. Here we report that a specific voltage-gated K^+ (K_V) channel subunit participates in very different K_V channels dominating the membrane conductances of type I and type II HCs in amniote vestibular organs.

Type I HCs occur only in amniote vestibular organs. Their most distinctive features are that they are enveloped by a calyceal afferent terminal (Wersäll, 1956; Lysakowski and Goldberg, 2004) and that they express $g_{K,L}$ (Correia and Lang, 1990; Rennie and Correia, 1994; Rüsch and Eatock, 1996a): a large non-inactivating conductance with an activation range from –100 to –60 mV, far more negative than other "low-voltage-activated" K_V channels. In addition to selectively attenuating and speeding up the receptor potentials of type I HCs (Correia et al., 1996; Rüsch and Eatock, 1996b), $g_{K,L}$ augments non-quantal transmission from type I hair cell to afferent calyx by providing open channels for K^+ flow into the synaptic cleft (Contini et al., 2012, 2017, 2020; Govindaraju et al., 2023), increasing the speed and linearity of the transmitted signal (Songer and Eatock, 2013).

Type II HCs have compact afferent synaptic contacts (boutons) where the receptor potential drives quantal release of glutamate. They have fast-inactivating (A-type, g_A) and delayed rectifier (g_{DR}) conductances that are opened by depolarization above resting potential (V_{rest}).

The unusual properties of $g_{K,L}$ have long attracted curiosity about its molecular nature. $g_{K,L}$ has been proposed to include "M-like" K_V channels in the K_V7 and/or erg channel families (Kharkovets et al., 2000; Hurley et al., 2006; Holt et al., 2007). The $K_V7.4$ subunit was of particular interest because it contributes to the low-voltage-activated conductance, $g_{K,n}$, in cochlear outer hair cells, but was eventually eliminated as a $g_{K,L}$ subunit by experiments on $K_V7.4$-null mice (Spitzmaul et al., 2013).

Several observations suggested the $K_V1.8$ (KCNA10) subunit as an alternative candidate for $g_{K,L}$. $K_V1.8$ is highly expressed in vestibular sensory epithelia (Carlisle et al., 2012), particularly hair cells (Lee et al., 2013; Scheffer et al., 2015; McInturff et al., 2018), with slight expression elsewhere (skeletal muscle, Lee et al., 2013; kidney, Yao, 2002). $K_V1.8^{-/-}$ mice show absent or delayed vestibular-evoked potentials, the synchronized activity of afferent nerve fibers sensitive to fast linear head motions (Lee et al., 2013). Unique among K_V1 channels, $K_V1.8$ has a cyclic nucleotide binding domain (Lang et al., 2000) with the potential to explain $g_{K,L}$'s known cGMP dependence (Behrend et al., 1997; Chen and Eatock, 2000).

Our comparison of whole-cell currents and immunohistochemistry in type I HCs from $K_V1.8^{-/-}$ and $K_V1.8^{+/+,+/-}$ mouse utricles confirmed that $K_V1.8$ expression is necessary for $g_{K,L}$. More surprisingly, $K_V1.8$ expression is also required for A-type and delayed rectifier conductances of type II HCs. In both HC types, eliminating the $K_V1.8$-dependent major conductances revealed a smaller delayed rectifier conductance involving K_V7 channels. Thus, the distinctive outward rectifiers that produce such different receptor potentials in type I and II HCs both include $K_V1.8$ and K_V7 channels.

Results

We compared whole-cell voltage-activated K^+ currents in type I and type II hair cells from homozygous knockout ($K_V1.8^{-/-}$) animals and their wildtype ($K_V1.8^{+/+}$) or heterozygote ($K_V1.8^{+/-}$) littermates. We immunolocalized $K_V1.8$ subunits in the utricular epithelium and pharmacologically characterized the residual K^+ currents of $K_V1.8^{-/-}$ animals. Current clamp experiments demonstrated the impact of $K_V1.8$-dependent currents on passive membrane properties.

We recorded from three utricular zones: lateral extrastriola (LES), striola, and medial extrastriola (MES) (Fig. 3A.1); striolar and extrastriolar zones have many structural and functional differences and give rise to afferents with different physiology (reviewed in Goldberg, 2000; Eatock and Songer, 2011). Recordings are from 412 type I and II HCs (53% LES, 30% MES, 17% striola) from mice between postnatal day (P) 5 and P370. We recorded from such a wide age range to test for developmental or senescent changes in the impact of the null mutation. Above P18, we did not see substantial changes in K_V channel properties, as reported (González-Garrido et al., 2021).

As reported (Lee et al., 2013), $K_V1.8^{-/-}$ animals appeared to be healthy and to develop and age normally.

$K_V1.8$ is necessary for $g_{K,L}$ in type I hair cells

The large low-voltage activated conductance, $g_{K,L}$, in $K_V1.8^{+/+,+/-}$ type I hair cells produces distinctive whole-cell current responses to voltage steps, as highlighted by our standard type I voltage protocol (Fig. 1A). From a holding potential within the $g_{K,L}$ activation range (here –74 mV), voltage steps to –124 mV, which is negative to E_K and the activation range, producing a large inward current through open $g_{K,L}$ channels that rapidly decays as the channels deactivate. The large transient inward current is a hallmark of $g_{K,L}$. Steady-state activation was measured from tail currents after iterated 500-ms step voltages (Fig. 1A)**.** We detected no difference between the Boltzmann parameters of $g_{K,L}$ G-V curves from $K_V1.8^{+/-}$ and $K_V1.8^{+/+}$ type I HCs.

For a similar voltage protocol, $K_V1.8^{-/-}$ type I HCs (Fig. 1B) produced no inward transient current at the step from –74 mV to –124 mV and much smaller depolarization-activated currents during the iterated steps, even at much more positive potentials. Figure 1C compares the conductance-voltage (G-V, activation) curves fit to tail currents (Eq. 1; see insets in Fig. 1A-B): the maximal conductance (g_{max}) of the $K_V1.8^{-/-}$ HC was over 10-fold smaller (Fig. 1C.1), and the curve was positively shifted by >40 mV (Fig. 1C.2). Figure 1D shows the G-V Boltzmann fit parameters for type I HCs from mice >P12, an age at which type I HCs normally express $g_{K,L}$ (Rüsch et al., 1998).

Suppl. Fig. 1 shows how G-V parameters of outwardly rectifying currents in type I HCs changed from P5 to P360. In $K_V1.8^{+/+,+,-}$ mice, the parameters transitioned over the first 15-20 postnatal days from values for a conventional delayed rectifier, activating positive to resting potential, to $g_{K,L}$ values, as previously described (Rüsch et al., 1998; Géléoc et al., 2004; Hurley et al., 2006). Between P5 and P10, we detected no evidence of a non-$g_{K,L}$ $K_V1.8$-dependent conductance in immature type I HCs (Suppl. Fig. 1B). In $K_V1.8^{-/-}$ type I HCs, $g_{K,L}$ was absent and G-V parameters did not change much with age from P5 to P370.

The much smaller residual delayed rectifier activated positive to resting potential, with V_{half} ~–40 mV and g_{max} density of 1.3 nS/pF. We characterize this $K_V1.8$-independent delayed rectifier later. A much larger non-$g_{K,L}$ delayed rectifier conductance ("$g_{DR,I}$") was reported in our earlier publication on mouse utricular type I HCs (Rüsch et al., 1998). This current was identified as that remaining after "blocking" $g_{K,L}$

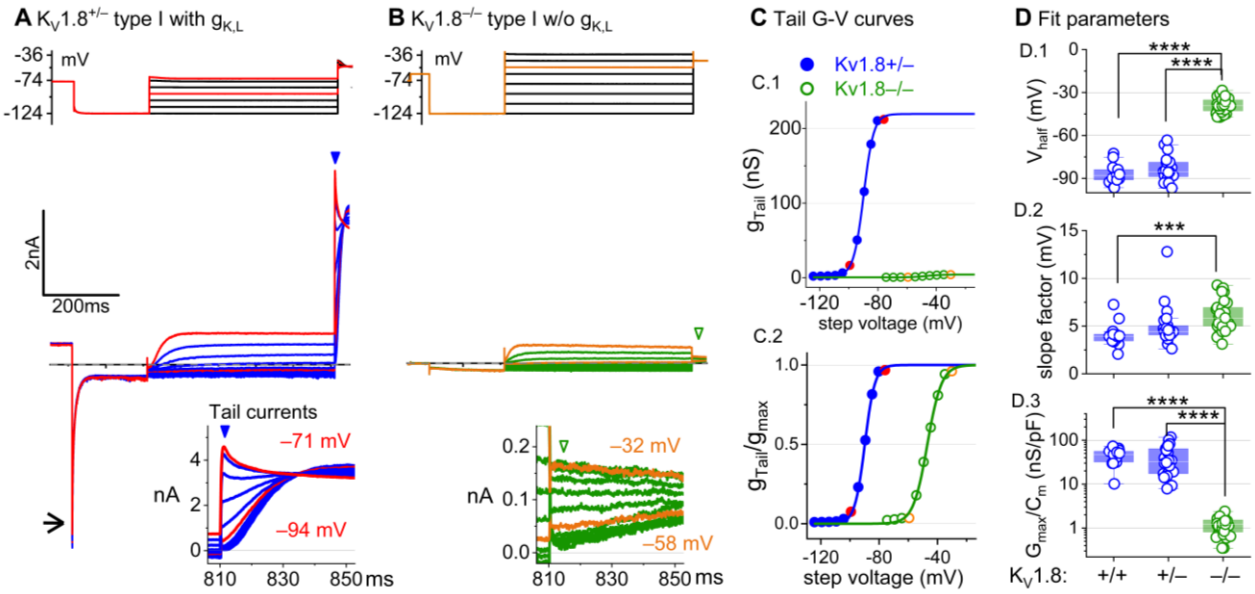

Figure 1. $K_V1.8^{-/-}$ type I hair cells lacked $g_{K,L}$, the dominant conductance in mature $K_V1.8^{+/+,+/-}$ type I HCs. Representative voltage-evoked currents in **(A)** a P22 $K_V1.8^{+/-}$ type I HC and **(B)** a P29 $K_V1.8^{-/-}$ type I HC. (A) *Arrow,* transient inward current that is a hallmark of $g_{K,L}$. Note that the voltage protocol (top) in B extends to more positive voltages. *Arrowheads,* tail currents, magnified in *insets*. **(C)** Activation (G-V) curves from tail currents in A and B; symbols, data; curves, Boltzmann fits (Eq. 1). **(D)** Fit parameters from mice >P12 show big effect of $K_V1.8^{-/-}$ and no difference between $K_V1.8^{+/-}$ and $K_V1.8^{+/+}$. *Asterisks* (here and elsewhere): *, p<0.05; **, p<0.01; ***, p<0.001; and ****, p<0.0001. *Line,* median; *Box,* interquartile range; *Whiskers*, outliers. See Table 1 for statistics.

with 20 mM external Ba^{2+}. Our new data suggest that there is no large non-$g_{K,L}$ conductance, and that instead high Ba^{2+} positively shifted the apparent voltage dependence of $g_{K,L}$.

$K_V1.8$ strongly affects type I passive properties and responses to current steps.

While the cells of $K_V1.8^{-/-}$ and $K_V1.8^{+/-}$ epithelia appeared healthy, type I hair cells had smaller membrane capacitances (C_m) and presumably surface areas: 4-5 pF in $K_V1.8^{-/-}$ type I HCs, ~20% smaller than $K_V1.8^{+/-}$ type I HCs (~6 pF) and ~30% smaller than $K_V1.8^{+/+}$ type I HCs (6-7 pF; Table 2). The decreased C_m may reflect deletion of a highly expressed trans-membrane protein (see discussion of $g_{K,L}$ channel density in Chen and Eatock, 2000, and for comparison the large decrease in outer hair cell size in the prestin null mutant (Liberman et al., 2002; Takahashi et al., 2018)).

Basolateral conductances help set the resting potential and passive membrane properties that regulate the time course and gain of voltage responses to small currents. To examine the effect of $K_V1.8$ on these properties, we switched to current clamp mode and measured resting potential (V_{rest}), input resistance (R_{in}, equivalent to voltage gain for small current steps, $\triangle V/\triangle I$), and membrane time constant (τ_{RC}). In $K_V1.8^{-/-}$ type I HCs, V_{rest} was much less negative (Fig. 2A.1), R_{in} was greater by ~20-fold (Fig. 2A.2), and membrane charging times were commensurately longer (Fig. 2A.3).

The differences between the voltage responses of $K_V1.8^{+/+,+/-}$ and $K_V1.8^{-/-}$ type I HCs are expected from the known impact of $g_{K,L}$ on V_{rest} and R_{in} (Correia and Lang, 1990; Ricci et al., 1996; Rüsch and Eatock, 1996b; Songer and Eatock, 2013). The large K^+-selective conductance at V_{rest} holds V_{rest} close to E_K (K^+ equilibrium potential) and minimizes gain ($\triangle V/\triangle I$), such that voltage-gated conductances are negligibly

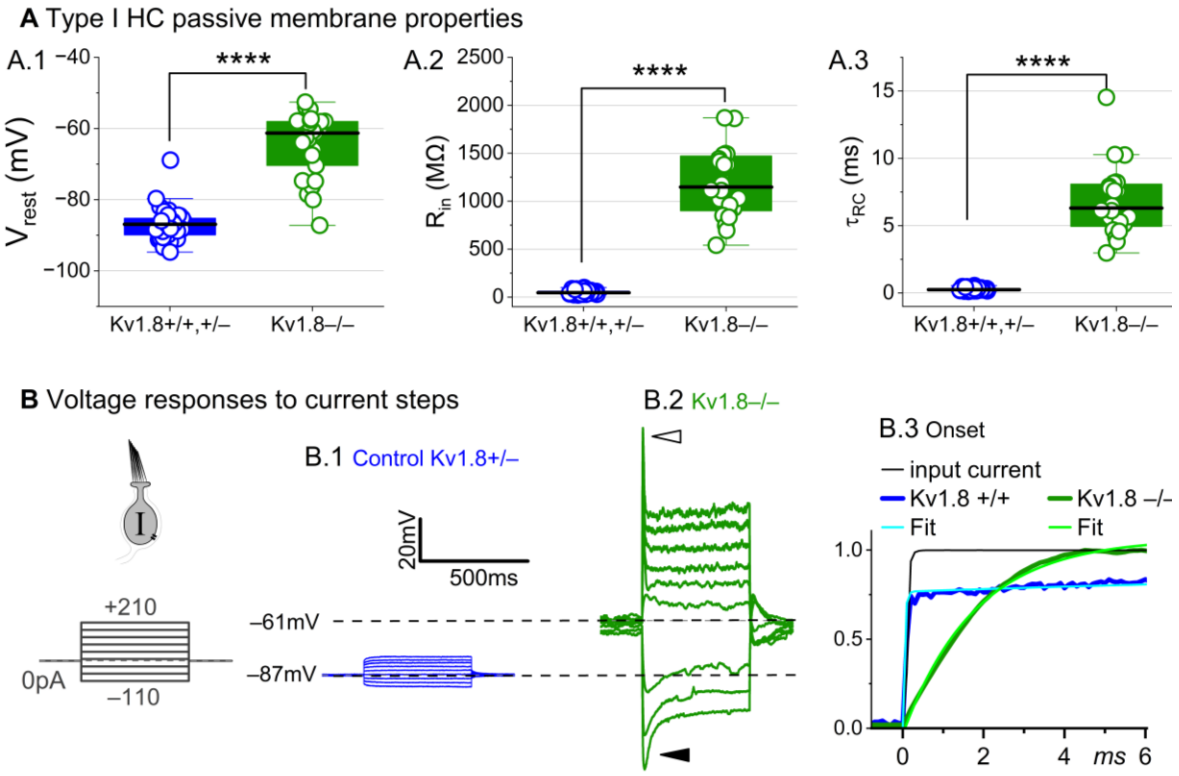

Figure 2. $K_V1.8^{-/-}$ type I hair cells had much longer membrane charging times and higher input resistances (voltage gains) than $K_V1.8^{+/+,+/-}$ type I HCs. (A) $g_{K,L}$ strongly affects passive membrane properties: (**A.1**) V_{rest} , (**A.2**) R_{in}, input resistance, and (**A.3**) membrane time constant, τ_{RC} = (R_{input} * C_m). See Table 2 for statistics. **(B)** Current clamp responses to the same scale from (B.1) $K_V1.8^{+/-}$ and (B.2) $K_V1.8^{-/-}$ type I cells, both P29. *Filled arrowhead (B.2),* sag indicating I_H activation. *Open arrowhead*, Depolarization rapidly decays as I_{DR} activates. B.3, The 1st 6 ms of voltage responses to 170-pA injection is normalized to steady-state value; overlaid curves are double-exponential fits ($K_V1.8^{+/+}$, τ 40 µs and 2.4 ms) and single-exponential fits ($K_V1.8^{-/-}$, τ 1.1 ms) .

affected by the input current and the cell produces approximately linear, static responses to iterated current steps. For $K_V1.8^{-/-}$ type I HCs, with their less negative V_{rest} and larger R_{in}, positive current steps evoked a fast initial depolarization (Fig. 2B.2), activating residual delayed rectifiers and repolarizing the membrane toward E_K. Negative current steps evoked an initial "sag" (Fig. 2B.2), a hyperpolarization followed by slow repolarization as the HCN1 channels open (Rüsch and Eatock, 1996b).

Overall, comparison of the $K_V1.8^{+/+,+/-}$ and $K_V1.8^{-/-}$ responses shows that with $K_V1.8$ ($g_{K,L}$), the voltage response of the type I hair cell is smaller but better reproduces the time course of the input current.

$K_V1.8$ is necessary for both inactivating and non-inactivating K_V currents in type II hair cells

Type II HCs also express $K_V1.8$ mRNA (McInturff et al., 2018; Orvis et al., 2021). Although their outwardly-rectifying conductances (g_A and g_{DR}) differ substantially in voltage dependence and size from $g_{K,L}$, both conductances were strongly affected by the null mutation: g_A was eliminated and the delayed rectifier

Table 1. *Type I hair cell K_V activation voltage dependence and kinetics. Mean ± SEM (number of cells). g is effect size, Hedge's g. KWA is Kruskal-Wallis ANOVA.*

Zone	$K_V1.8$	Tail $V_{1/2}$, mV [a]	Tail S, mV [b]	Tail G_{max}, nS [c]	Tail G_{max}/C_m, nS/pF [d]	Age (median, range)
Extrastriola	+/+	–85 ± 2 (12)	4.3 ± 0.4 (12)	270 ± 40 (11)	47 ± 8 (11)	22, 14-287
	+/–	–83 ± 1 (40)	5.2 ± 0.3 (40)	210 ± 20 (40)	37 ± 4 (40)	19, 13-259
	–/–	–40.2 ± 0.9 (26)	5.7 ± 0.3 (26)	5.4 ± 0.3 (26)	1.11 ± 0.08 (26)	45, 14-277
Striola	+/+	–87 ± 3 (6)	4.3 ± 0.3 (6)	310 ± 70 (6)	41 ± 7 (6)	40, 15-59
	+/–	–88 ± 2 (3)	4.7 ± 0.9 (3)	270 ± 60 (3)	44 ± 6 (3)	19, 14-20
	–/–	–38 ± 1 (13)	6.2 ± 0.4 (13)	6.5 ± 0.6 (13)	1.5 ± 0.1 (13)	202, 14-370

[a] –/– vs +/+: 2-way ANOVA, p < 1E-9, g 7.7; –/– vs +/–: 2-way ANOVA, p < 1E-9, g 6.8
[b] –/– vs +/+: 2-way ANOVA, p = 8.4E-4, g 1.2
[c] –/– vs +/+: 2-way ANOVA, p < 1E-9, g 3.7; –/– vs +/–: 2-way ANOVA, p < 1E-9, g 2.1
[d] –/– vs +/+: 2-way ANOVA, p < 1E-9, g 3.6; –/– vs +/–: 2-way ANOVA, p < 1E-9, g 2.0

Table 2. *Type I hair cell* passive *membrane properties. Mean ± SEM (number of cells). g is effect size, Hedge's g. KWA is Kruskal-Wallis ANOVA.*

Zone	*$K_V1.8$*	*V_{rest}, mV* [a, b]	R_{input}, MΩ [c]	τ_{RC}, ms [d]	C_m (pF) [e]	Age (median, range)
Extrastriola	+/+	–84 ± 3 (6)	44 ± 6 (6)	0.24 ± 0.03 (6)	6.1 ± 0.4 (13)	19.5, 14-287
	+/–	–88.0 ± 0.7 (28)	55 ± 5 (24)	0.32 ± 0.03 (23)	5.8 ± 0.2 (44)	21, 16-29
	–/–	–63 ± 2 (15)	1400 ± 100 (15)	6.4 ± 0.6 (15)	5 ± 0.2 (27)	45, 14-202
Striola	+/+	–87 ± 2 (4)	50 ± 8 (4)	0.30 ± 0.04 (4)	7.4 ± 0.7 (7)	43, 40-59
	+/–	–87 ± 3 (3)	38 ± 8 (2)	0.21 ± 0.01 (2)	5.9 ± 0.6 (3)	19, 19-20
	–/–	–74 ± 5 (5)	1000 ± 300 (4)	4.2 ± 1.0 (4)	4.4 ± 0.2 (14)	202, 24-370

[a] striolar –/– vs ES –/–: 2-way ANOVA, p = 0.006, g 1.2; striolar –/– vs striolar +/+,+/–: 2-way ANOVA, p = 0.005, g 1.7
[b] –/– vs +/+: 2-way ANOVA, p < 1E-9, g 2.3; –/– vs +/–: 2-way ANOVA, p < 1E-9, g 3.4
[c] –/– vs +/+: 2-way ANOVA, p < 1E-9, g 3.1; –/– vs +/–: 2-way ANOVA, p < 1E-9, g 3.9
[d] –/– vs +/+: 2-way ANOVA, p < 1E-9, g 2.7; –/– vs +/–: 2-way ANOVA, p < 1E-9, g 3.4
[e] –/– vs +/+: 2-way ANOVA, p = 3E-7, g 1.5; –/– vs +/–: 2-way ANOVA, p = 1.3E-4, g 1.0; +/– vs +/+: 2-way ANOVA, p = 0.048, g 0.6

was substantially smaller. Below we describe g_A and g_{DR} in $K_V1.8^{+/+,+/-}$ type II HCs and the residual outward rectifying current in $K_V1.8^{-/-}$ type II HCs.

$K_V1.8^{+/+,+/-}$ type II HCs. Most (81/84) $K_V1.8^{+/+,+/-}$ type II HCs expressed a rapidly-activating, rapidly-inactivating A-type conductance (g_A). We define A current as the outwardly rectifying current that

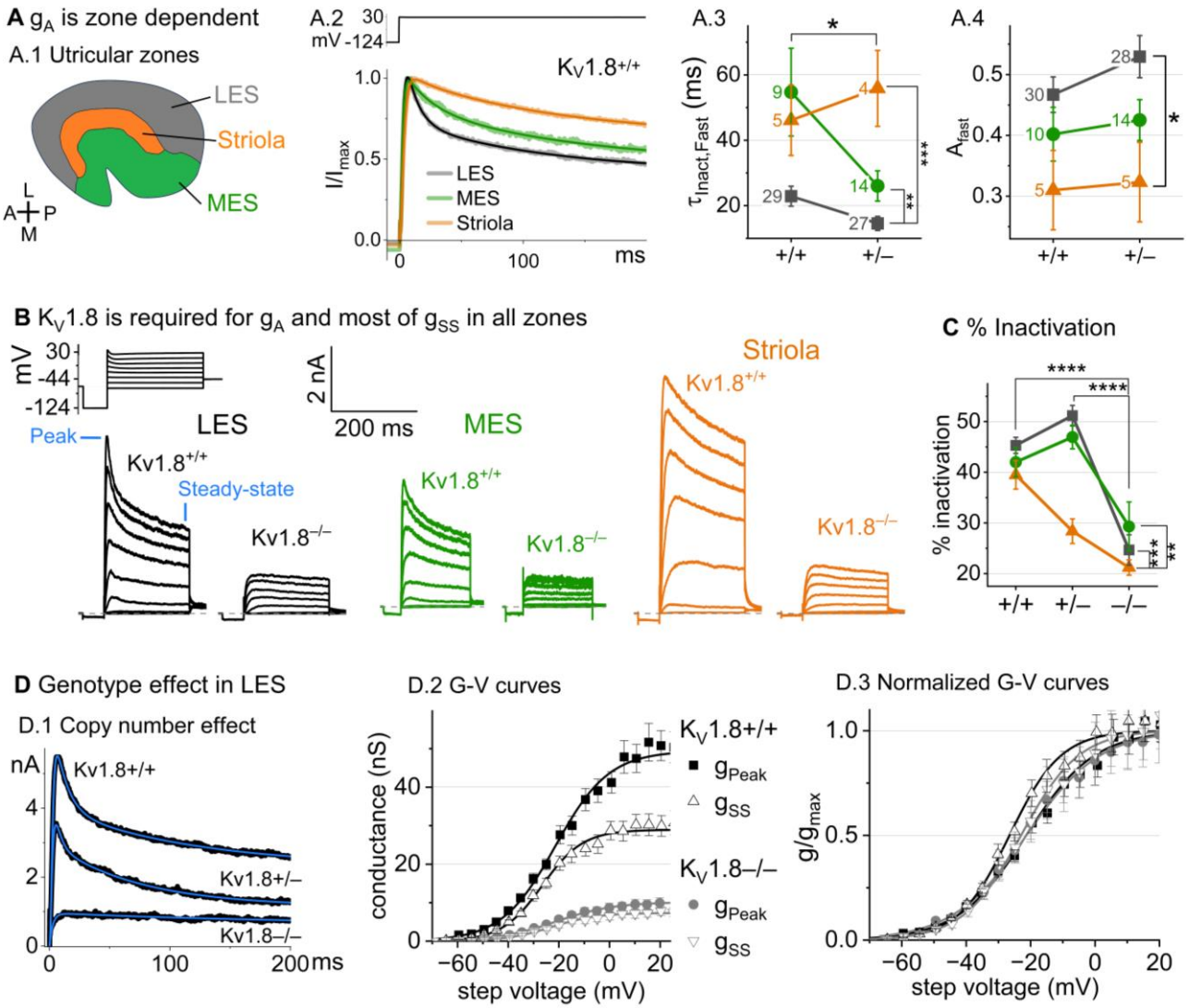

Figure 3. $K_V1.8^{-/-}$ type II HCs in all zones of the sensory epithelium lacked the major rapidly inactivating conductance, g_A, and had less delayed rectifier conductance. Activation and inactivation varied with epithelial zone and genotype. (**A**) g_A inactivation time course varied across zones. (**A.1**) Zones of the utricular epithelium. (**A.2**) Normalized currents evoked by steps from –124 mV to +30 mV with overlaid fits of Eq. 3. (**A.3**) $\tau_{Inact,Fast}$ was faster in $K_V1.8^{+/-}$ than $K_V1.8^{+/+}$ HCs , and faster in LES than other zones. Brackets show post hoc pairwise comparisons between two zones (vertical brackets) and horizontal brackets compare two genotypes; see Table 3 for statistics. (**A.4**) Fast inactivation was a greater fraction of total inactivation in LES than striola.
(**B**) Exemplars; ages, *left to right*, P312, P53, P287, P49, P40, P154.
(**C**) % inactivation at 30 mV was much lower in $K_V1.8^{-/-}$ than $K_V1.8^{+/-}$ and $K_V1.8^{+/+}$, and lower in striola than LES and MES. Interaction between zone and genotype was significant (Table 3).
(**D**) Exemplar currents and G-V curves from LES type II HCs show a copy number effect. (**D.1**) Currents for examples of the 3 genotypes evoked by steps from –124 mV to +30 mV fit with Eq. 3. (**D.2**) Averaged peak and steady-state conductance-voltage datapoints from LES cells (+/+, n=37; –/–, n=20) were fit with Boltzmann equations (Eq. 1) and normalized by g_{max} in (**D.3**). See Table 4 for statistics.

inactivates by over 30% within 200 ms. g_A was more prominent in extrastriolar zones, as reported (Holt et al. 1999, Weng and Correia 1999).

We compared the activation and inactivation time course and inactivation prominence for 200-ms steps from –124 mV to ~30 mV. Outward currents fit with Eq. 3 yielded fast inactivation time constants

($\tau_{Inact, Fast}$) of ~30 ms in LES (Fig. 3A.2). $\tau_{Inact, Fast}$ was faster in LES than in MES or striola (Fig. 3A.3) and fast inactivation was a larger fraction of the total inactivation in LES than striola (~0.5 vs. 0.3, Fig. 3A.4).

To show voltage dependence of activation, we generated G-V curves for peak currents (sum of A-current and delayed rectifier) and steady-state currents measured at 200 ms, after g_A has mostly inactivated (Figure 3D.2). $K_V1.8^{+/-}$ HCs had smaller currents than $K_V1.8^{+/+}$ HCs, reflecting a smaller g_{DR} (Fig. 3D) and faster fast inactivation (Fig. 3A.3). As discussed later, these effects may relate to effects of the $K_V1.8$ gene dosage on the relative numbers of different $K_V1.8$ heteromers.

For $K_V1.8^{+/+}$ and $K_V1.8^{+/-}$ HCs, the voltage dependence as summarized by V_{half} and slope factor (S) was similar. Relative to g_{SS}, g_{Peak} had a more positive V_{half} (~–21 vs. ~–26) and greater S (~12 vs. ~9, Fig. 3D, Table 4). Because g_{Peak} includes channels with and without fast inactivation, the shallower g_{Peak}-V curve may reflect a more heterogeneous channel population. Only g_{Peak} showed zonal variation, with more positive V_{half} in LES than striola (~–20 mV vs. ~–24 mV, Fig. 3D, Table 4). We later suggest that variable subunit composition may drive zonal variation in g_{Peak}.

$K_V1.8^{-/-}$ type II HCs from all zones were missing g_A and 30-50% of g_{DR} (Fig. 3B-D). The residual delayed rectifier (1.3 nS/pF) had a more positive V_{half} than g_{DR} in $K_V1.8^{+/+,+/-}$ HCs (~–20 mV *vs.* ~–26 mV, Fig. 3D.2). We refer to the $K_V1.8$-dependent delayed rectifier component as $g_{DR}(K_V1.8)$ and to the residual, $K_V1.8$-*in*dependent delayed rectifier component as $g_{DR}(K_V7)$ because, as we show later, it includes K_V7 channels.

Supplemental Figure 3A shows the development of $K_V1.8$-dependent and independent K_V currents in type II HCs with age from P5 to over P300. In $K_V1.8^{+/+,+/-}$ type II HCs, g_A was present at all ages with a higher % inactivation after P18 than at P5-P10 (Suppl. Fig. 3A.4). g_{Peak} did not change much above P12 except for a compression of conductance density from P13 to P370 (partial correlation coefficient = –0.4, p = 2E-5, Suppl. Fig. 3A.3).

We saw small rapidly inactivating outward currents in a minority of $K_V1.8^{-/-}$ type II HCs (23%, 7/30), all >P12 and extrastriolar (Suppl. Fig. 4). These currents overlapped with g_A in percent inactivation, inactivation kinetics, and activation voltage dependence but were very small. As discussed later, we suspect that these currents flow through homomers of inactivating K_V subunits that in control hair cells join with $K_V1.8$ subunits and confer inactivation on the heteromeric conductance.

$K_V1.8$ affects type II passive properties and responses to current steps.

In type II HCs, absence of $K_V1.8$ did not change V_{rest} (Fig. 4A.1) because g_A and g_{DR} both activate positive to rest, but significantly increased R_{in} and τ_{RC} (Fig. 4A.2-A.3).

Positive current steps evoked an initial depolarizing transient in both $K_V1.8^{+/+}$ and $K_V1.8^{-/-}$ type II HCs, but the detailed time course differed (Fig. 4B). Both transient and steady-state responses were larger in $K_V1.8^{-/-}$, consistent with their larger R_{in} values.

Table 3. *Type II hair cell K_V currents: Activation and inactivation time course at +30 mV. Mean ± SEM. g is effect size, Hedge's g. KWA is Kruskal-Wallis ANOVA.*

Zone	$K_V1.8$	τ_{Act} at 30 mV, ms [a, b]	$\tau_{Inact,Fast}$ at 30 mV, ms [c, d]	Fast inactivation prominence [e]	Inactivation % [f, g]	N cells	Age (median, range)
LES	+/+	2.11 ± 0.09	23 ± 3	0.46 ± 0.03	45 ± 2	30	46, 14-312
	+/–	1.64 ± 0.09	15 ± 2	0.53 ± 0.03	51 ± 2	27	29, 13-280
	–/–	4.4 ± 0.5	*NA*	*NA*	25 ± 3	21	128, 15-355
MES	+/+	2.8 ± 0.5	50 ± 10	0.40 ± 0.04	42 ± 3	9	94, 22-296
	+/–	2.2 ± 0.2	90 ± 60	0.42 ± 0.03	47 ± 2	15	24, 13-52
	–/–	10 ± 7	*NA*	*NA*	29 ± 5	10	84, 28-355
Striola	+/+	2.7 ± 0.3	50 ± 10	0.31 ± 0.07	39 ± 3	5	45, 40-287
	+/–	2.9 ± 0.4	300 ± 200	0.3 ± 0.06	28 ± 2	5	19, 14-30
	–/–	7 ± 2	*NA*	*NA*	22 ± 2	6	202, 29-298

[a] –/– vs +/+: KWA, p = 0.0048, g 0.6; –/– vs +/–: KWA, p = 2.3E-7, g 0.6
[b] Striola vs LES: KWA, p = 5.7E-4, g 1.0
[c] +/– vs +/+: KWA, p = 0.027, g 0.2
[d] LES vs MES: KWA, p = 0.0018, g 0.3; LES vs Striola: KWA, p = 1.9E-4, g 0.8
[e] LES vs Striola: 2-way ANOVA, p = 0.0041, g 0.7
[f] –/– vs +/+: 2-way ANOVA, p < 1E-9, g 1.7; –/– vs +/–: 2-way ANOVA, p < 1E-9, g 1.8
[g] Striola vs LES: 2-way ANOVA, p = 3.4E-5, g 0.9; Striola vs MES: 2-way ANOVA, p = 0.0011, g 1.0; Interaction between genotype and Zone: 2-way ANOVA, p = 0.026

Table 4. *Type II hair cell K_V currents: Activation voltage dependence. Mean ± SEM. g is effect size, Hedge's g. KWA is Kruskal-Wallis ANOVA.*

Zone	*$K_V1.8$*	*Peak $V_{1/2}$, mV* [a]	Peak S, mV [b, c]	A-type g_{max}/C_m, nS/pF [d]	SS V_{half}, mV [e]	SS S, mV [f]	SS g_{max}/C_m, nS/pF [g, h]	N cells	Age (median, range)
LES	+/+	–19.8 ± 0.6	11.8 ± 0.4	4.0 ± 0.3	–25.0 ± 0.5	8.7 ± 0.3	7.1 ± 0.8	37	46, 14-312
	+/–	–19.8 ± 0.8	12.8 ± 0.4	3.8 ± 0.3	–26.8 ± 0.8	8.7 ± 0.3	4.9 ± 0.4	35	29, 13-280
	–/–	–18 ± 1	11.7 ± 0.4	0.37 ± 0.05	–19 ± 1	12.1 ± 0.5	1.8 ± 0.2	20	128, 15-355
MES	+/+	–22 ± 1	11 ± 0.7	4.1 ± 0.7	–26 ± 1	8.3 ± 0.5	9 ± 1	11	94, 22-296
	+/–	–21 ± 1	11.8 ± 0.4	3.6 ± 0.5	–27 ± 1	9.0 ± 0.3	5.9 ± 0.7	16	24, 13-52
	–/–	–19 ± 1	10.8 ± 0.6	0.6 ± 0.1	–20 ± 1	10.7 ± 0.7	2.5 ± 0.3	15	84, 28-355
Striola	+/+	–24 ± 1	9.6 ± 0.5	5 ± 1	–26.6 ± 0.9	8.2 ± 0.4	12 ± 1	7	45, 40-287
	+/–	–25 ± 2	9.4 ± 0.4	2.6 ± 0.6	–28 ± 2	8.2 ± 0.3	10 ± 2	6	19, 14-30
	–/–	–21.3 ± 0.9	10.3 ± 0.5	0.7 ± 0.1	–21.7 ± 0.8	10.5 ± 0.6	3.9 ± 0.5	8	202, 29-298

[a] Striola vs LES: 2-way ANOVA, p = 0.00116, g 0.9
[b] Striola vs MES: 2-way ANOVA, p = 0.016, g 0.8; Striola vs LES: 2-way ANOVA, p = 7.5E-6, g 1.2
[c] –/– vs +/–: 2-way ANOVA, p = 0.036, g 0.5
[d] –/– vs +/+: Welch ANOVA, p < 1E-9, g 2.3; –/– vs +/–: Welch ANOVA, p < 1E-9, g 2.3
[e] –/– vs +/+: 2-way ANOVA, p < 1E-9, g 1.4; –/– vs +/–: 2-way ANOVA, p < 1E-9, g 1.6
[f] –/– vs +/+: 2-way ANOVA, p < 1E-9, g 1.4; –/– vs +/–: 2-way ANOVA, p = 4.5E-7, g 1.1
[g] –/– vs +/+: Welch ANOVA, p < 1E-9, g 1.6; –/– vs +/–: Welch ANOVA, p < 1E-9, g 1.3; +/+ vs +/–: Welch ANOVA, p = 0.007, g 1.6
[h] Striola vs LES: 1-way ANOVA, p = 0.001, g 0.9); Striola vs MES: 1-way ANOVA, p = 0.01, g 0.8

223

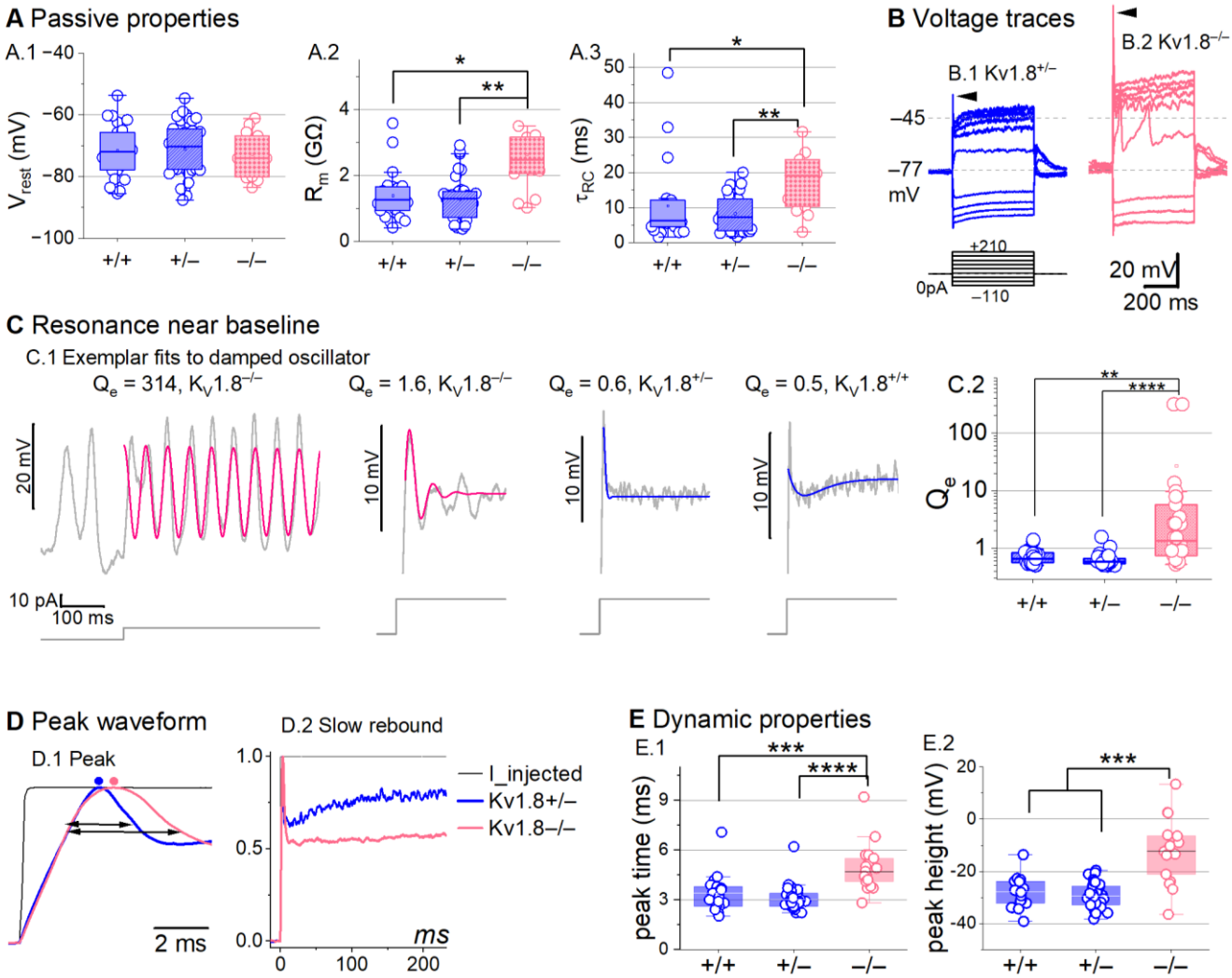

Figure 4. $K_V1.8^{-/-}$ type II hair cells had larger, slower voltage responses and more electrical resonance. **(A)** Passive membrane properties near resting membrane potential: A.1) Resting potential. R_{input} (A.2) and τ_{RC} (A.3) were obtained from single exponential fits to voltage responses < 15 mV. See Table 5 for statistics.
(**B**) Exemplar voltage responses to iterated current steps (*bottom)* illustrate key changes in gain and resonance with $K_V1.8$ knockout. (**B.1**) $K_V1.8^{+/-}$ type II HC (P24, LES) and (**B.2**) $K_V1.8^{-/-}$ type II HC (P53, LES). *Arrowheads,* depolarizing transients.
(**C**) Range of resonance illustrated for $K_V1.8^{-/-}$ type II HCs (*left, pink curves fit to Eq. 5*) and controls (*right, blue fits*). (**C.1**) *Resonant frequencies, left to right:* 19.6, 18.4, 34.4, 0.3 Hz. Leftmost cell resonated spontaneously (before step). (**C.2**) Tuning quality (Q_e; Eq. 6) was higher for $K_V1.8^{-/-}$ type II HCs (KWA, p = 0.0064 vs. $K_V1.8^{+/+}$; p = 7E-8 vs. $K_V1.8^{+/-}$).
(**D**) $K_V1.8^{-/-}$ type II HCs had higher, slower peaks and much slower rebound potentials in response to large (170-pA) current steps. (**D.1**) Normalized to show initial depolarizing transient (*filled circles*, times of peaks; *horizontal arrows*, peak width at half-maximum). (**D.2**) Longer time scale to highlight how null mutation reduced post-transient rebound.
(**E**) In $K_V1.8^{-/-}$ HCs, depolarizing transients evoked by a +90-pA step were slower to peak (**E.1**) and (**E.2**) larger.

Absence of $K_V1.8$ increased the incidence of sharp electrical resonance in type II HCs. Electrical resonance, which manifests as ringing responses to current steps, can support receptor potential tuning (Ashmore, 1983; Fettiplace, 1987; Hudspeth and Lewis, 1988; Ramanathan and Fuchs, 2002). Larger R_{in} values made $K_V1.8^{-/-}$ type II HCs more prone to electrical resonance; Figure 4C.1 shows a striking example. Median resonance quality (Q_e, sharpness of tuning) was greater in $K_V1.8^{-/-}$ (1.33, n=26) than $K_V1.8^{+/+}$ (0.66, n=23) or $K_V1.8^{+/-}$ (0.59, n=44) type II HCs.

Table 5. *Type II hair cell passive membrane properties. Mean ± SEM (number of cells). g is effect size, Hedge's g. KWA is Kruskal-Wallis ANOVA.*

Zone	$K_V1.8$	V_{rest}, mV	R_{input}, GΩ [a]	τ_{RC}, ms [b]	Peak height, mV, 170 [c]	Peak time, ms [d]	C_m, pF	Age (median, range)
Extrastriola	+/+	–71 ± 2 (19)	1.4 ± 0.2 (16)	11 ± 3 (16)	–20 ± 2 (15)	2.5 ± 0.2 (15)	4.7 ± 0.2 (50)	45, 16-312
	+/–	–71 ± 2 (34)	1.2 ± 0.1 (27)	9 ± 1 (27)	–20 ± 1 (30)	2.44 ± 0.08 (30)	4.6 ± 0.1 (52)	27, 13-280
	–/–	–76 ± 2 (9)	2.3 ± 0.3 (7)	16 ± 3 (7)	2 ± 6 (7)	3.6 ± 0.3 (7)	4.6 ± 0.2 (35)	53, 15-154
Striola	+/+	–73.1 ± 1.0 (6)	1.4 ± 0.1 (6)	9 ± 1 (6)	–20 ± 2 (5)	2.7 ± 0.1 (5)	4.6 ± 0.2 (7)	45, 40-224
	+/–	–71 ± 3 (5)	1.4 ± 0.3 (6)	7 ± 2 (6)	–20 ± 2 (6)	2.3 ± 0.1 (6)	4.8 ± 0.2 (6)	19, 19-30
	–/–	–68 ± 2 (6)	3.0 ± 0.7 (6)	26 ± 10 (6)	2 ± 7 (4)	4 ± 1 (4)	4.4 ± 0.3 (7)	178, 29-298

[a] –/– vs +/+: KWA, p = 0.015, g 1.2; –/– vs +/–: KWA, p = 0.002, g 1.5
[b] –/– vs +/+: KWA, p = 0.016, g 0.7; –/– vs +/–: KWA, p = 0.008, g 1.2
[c] –/– vs +/+: KWA, p = 0.006, g 2.1; –/– vs +/–: KWA, p = 2E-4, g 2.6
[d] –/– vs +/+: 2-way ANOVA, p <1E-9, g 1.3; –/– vs +/–: 2-way ANOVA, p < 1E-9, g 1.9

$K_V1.8$ affected the time course of the initial peak in response to much larger current injections (Fig. 4D-E). Fast activation of g_A in control type II HCs rapidly repolarizes the membrane and then inactivates, allowing the constant input current to progressively depolarize the cell, producing a slow rebound (Fig 4D.2). This behavior has the potential to counter MET adaptation (Vollrath and Eatock, 2003).

$K_V1.8$ immunolocalized to basolateral membranes of both type I and II HCs

If $K_V1.8$ is a pore-forming subunit in the $K_V1.8$-dependent conductances $g_{K,L}$, g_A, and g_{DR}, it should localize to hair cell membranes. Figure 5 compares $K_V1.8$ immunoreactivity in $K_V1.8^{+/+}$ and $K_V1.8^{-/-}$ utricles, showing specific immunoreactivity along the basolateral membranes of both hair cell types in $K_V1.8^{+/+}$ utricles. To identify hair cell type and localize the hair cell membrane, we used antibodies against $K_V7.4$ (KCNQ4), an ion channel densely expressed in the calyceal "inner-face" membrane next to the synaptic cleft (Hurley et al., 2006; Lysakowski et al., 2011), producing a cup-like stain around type I HCs (Fig. 5A). $K_V1.8$ immunoreactivity was present in hair cell membrane apposing $K_V7.4$-stained calyx inner face in $K_V1.8^{+/+}$ utricles (Fig. 5A.1, A.2) and not in $K_V1.8^{-/-}$ utricles (Fig. 5A.3).

In other experiments, we used antibodies against calretinin (Calb2), a cytosolic calcium binding protein expressed by many type II HCs and also by striolar calyx-only afferents (Desai et al., 2005; Lysakowski et al., 2011) (Fig. 5B). A hair cell is type II if it is calretinin-positive (Fig. 5B.1) or if it lacks a $K_V7.4$-positive or

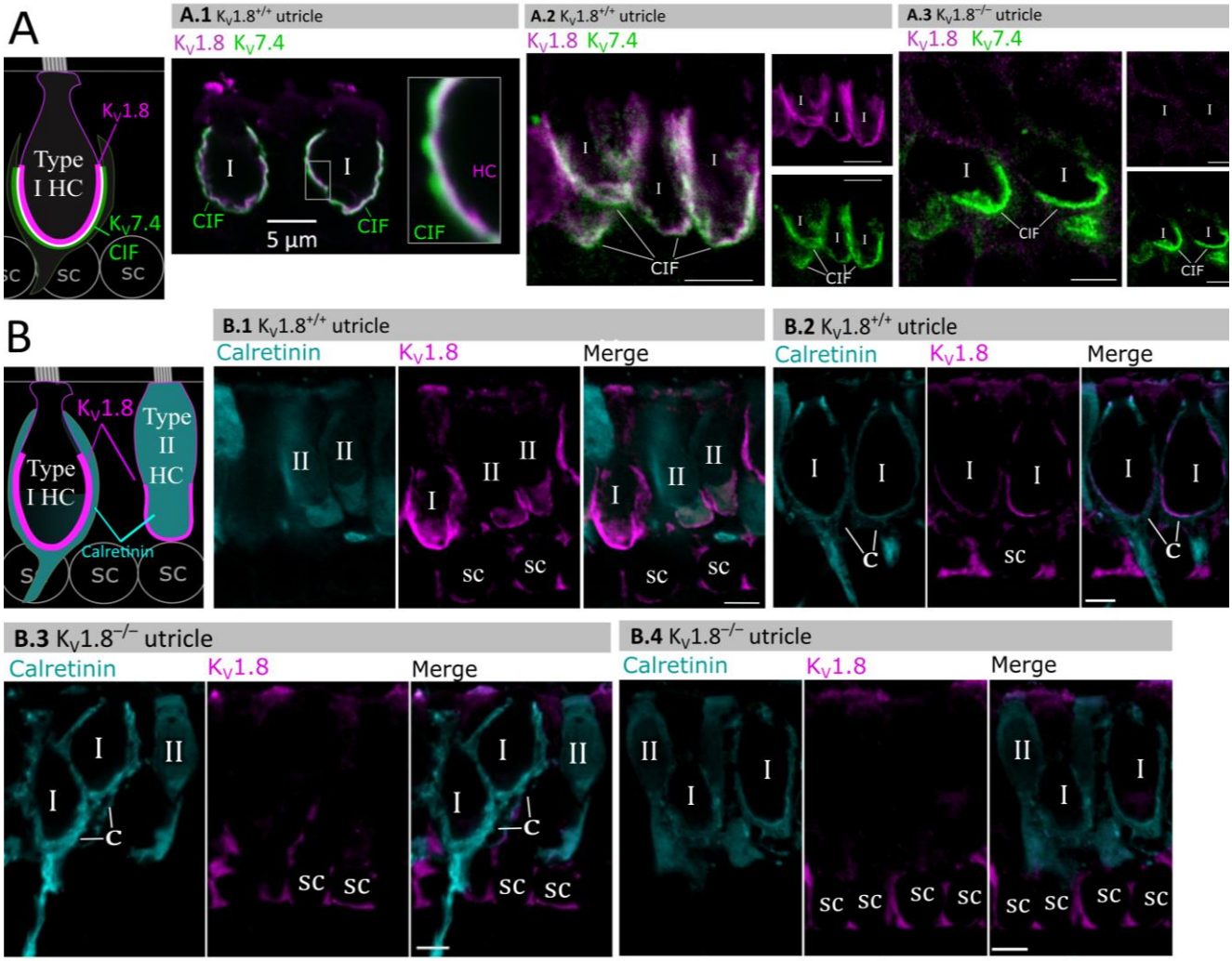

Figure 5. **Type I and type II HC basolateral membranes show specific immunoreactivity to Kv1.8 antibody (magenta).** Antibodies for $K_V7.4$ (A, green) and calretinin (B, cyan) were used as counterstains for calyx membrane (Kv7.4), type II HC cytoplasm (calretinin) and cytoplasm of striolar calyx-only afferents (calretinin). (**A**) *Left,* Cartoon showing $K_V7.4$ on the calyx inner face membrane (CIF) and $K_V1.8$ on the type I HC membrane. SC, supporting cell nuclei. *A.1-3*, Adult mouse utricle sections. $K_V7.4$ antibody labeled calyces on two $K_V1.8$-positive type I HCs (**A.1**), four $K_V1.8$-positive type I HCs (**A.2**), and two $K_V1.8$-negative type I HCs from a $K_V1.8^{-/-}$ mouse (**A.3**). (**B**) *Left,* Cartoon showing cytoplasmic calretinin stain in calyx-only striolar afferents and most type II HCs, and $K_V1.8$ on membranes of both HC types. In wildtype utricles, $K_V1.8$ immunolocalized to basolateral membranes of type I and II HCs (**B.1**). $K_V1.8$ immunolocalized to type I HCs in striola (**B.2**). Staining of supporting cell (SC) membranes by Kv1.8 antibody was non-specific, as it was present in $K_V1.8^{-/-}$ tissue (**B.3, B.4**).

calretinin-positive calyceal cup (Fig. 5A.2, 5B.3, rightmost cells). Hair cell identification was confirmed with established morphological indicators: for example, type II HCs tend to have basolateral processes (feet) (Pujol et al., 2014) and, in the extrastriola, more apical nuclei than type I HC.

Previously, Carlisle et al. (2012) reported $K_V1.8$-like immunoreactivity in many cell types in the inner ear. In contrast, Lee et al. (2013) found that gene expression reporters indicated expression only in hair cells and some supporting cells. Here, comparison of control and null tissue showed selective expression of HC membranes, and that some supporting cell staining is non-selective.

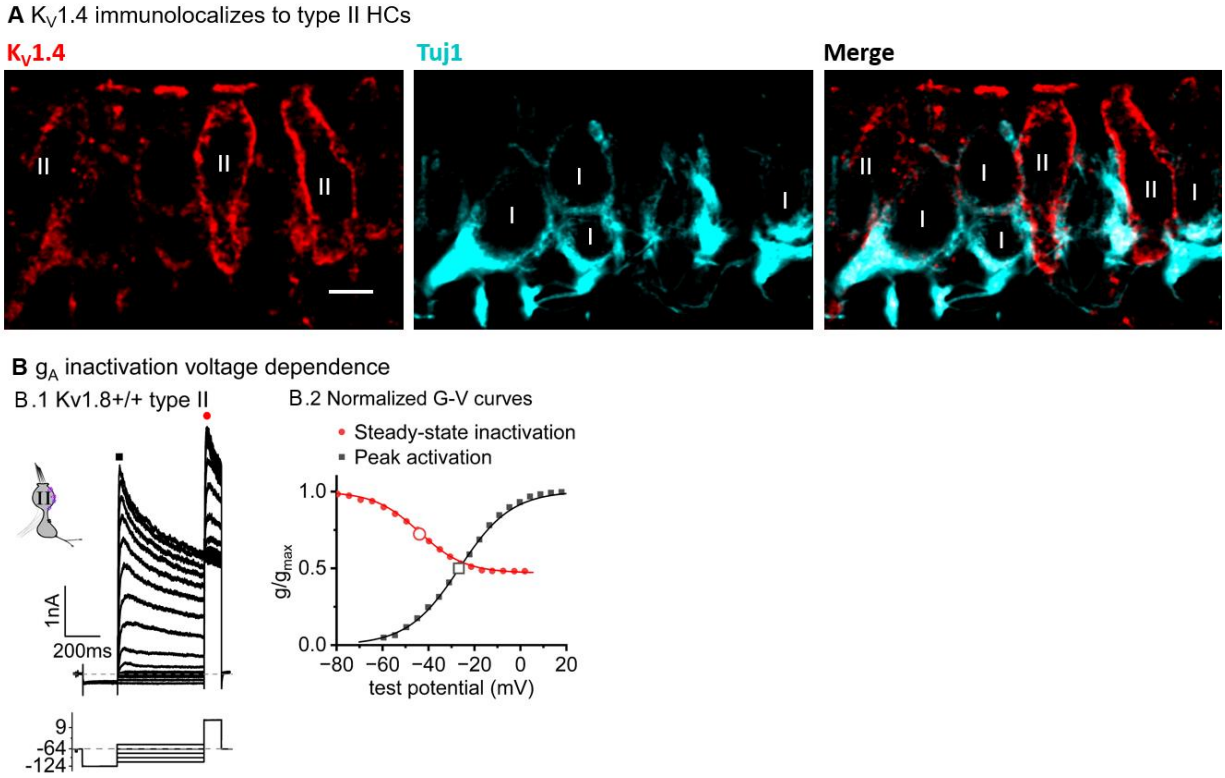

Figure 6. **K_V1.4 subunits may contribute to g_A in extrastriolar type II HCs**.
(**A**) Immunostaining of adult rat utricular epithelium with K_V1.4 antibody and TUJ-1, which labels afferent terminals, shows strong K_V1.4-like immunoreactivity on the membranes of 2 type II HCs. *Scale bar,* 5 µm.
(**B**) Voltage dependence of g_A's steady-state inactivation (h_∞ curve) and peak activation are consistent with K_V1.4 heteromers. $K_V1.8^{+/+,+/-}$ type II HCs, n=11, P40-P210, median P94. (**B.1**) The inactivation voltage protocol, bottom. Tail current is a function of the voltage dependence of accumulated steady-state inactivation. 100 µM ZD7288 in bath prevented contamination by HCN current. (**B.2**) Overlapping normalized activation and inactivation ("h-infinity") G-V curves for data in B.1 at time points shown: peak currents (black squares, activation) and tail currents (red circles, inactivation). *Curves,* Boltzmann fits (Eq. 1). Average fit parameters for inactivation: V_{half}, –42 ±2 mV (n=11); S, 11 ± 1 mV. Activation: V_{half}, –23 ± 1 mV (n=11); S, 11.2 ± 0.4 mV.

K_V1.4 may also contribute to g_A

Results with the K_V1.8 knockout suggest that type II hair cells have an inactivating K_V1 conductance that includes K_V1.8 subunits. K_V1.8, like most K_V1 subunits, is not inactivating as a heterologously expressed homomer (Lang et al., 2000; Ranjan et al., 2019; Dierich et al., 2020), nor are the K_V1.8-dependent channels in type I HCs, as we show, and cochlear inner hair cells (Dierich et al., 2020). K_V1 subunits without intrinsic inactivation can produce rapidly inactivating currents by associating with $K_V\beta$1 (KCNB1) or $K_V\beta$3 subunits. $K_V\beta$1 is present in type II HCs alongside $K_V\beta$2 (McInturff et al., 2018; Jan et al., 2021; Orvis et al., 2021), which does not confer rapid inactivation (Dwenger et al., 2022).

An alternative possibility is that in type II HCs, K_V1.8 subunits heteromultimerize with K_V1.4 subunits – the only K_V1 subunits which, when expressed as a homomer, have complete N-type (fast) inactivation (Stühmer et al., 1989). Multiple observations support this possibility. K_V1.4 has been linked to g_A in pigeon type II HCs (Correia et al., 2008) and is the second-most abundant K_V1 transcript in mammalian vestibular HCs, after K_V1.8 (Scheffer et al., 2015). K_V1.4 is expressed in type II HCs but not type I HCs (McInturff et

al., 2018; Orvis et al., 2021), and is not found in striolar HCs (Jan et al., 2021; Orvis et al., 2021), where even in type II HCs, inactivation is slower and less extensive (Fig. 3A).

In $K_V1.8^{+/+,+/-}$ type II HCs, the time course (Fig. 3A, $\tau_{Fast,Inac}$ of ~30 ms +30 mV) and voltage dependence of inactivation of g_A (V_{half} –41 mV, Fig. 6B.2), are consistent with heterologously expressed heteromers of $K_V1.4$ with $K_V1.x$ and/or $K_V\beta1$ (Imbrici et al., 2006; Al-Sabi et al., 2011). In further support, we observed $K_V1.4$-like immunoreactivity along the basolateral membranes of extrastriolar type II HCs in rat utricles (Fig. 6A).

K_V7 channels contribute a small delayed rectifier in type I and type II hair cells

In $K_V1.8^{-/-}$ HCs, absence of $I_{K,L}$ and I_A revealed smaller delayed rectifier K^+ currents that, unlike $I_{K,L}$, activated positive to resting potential and, unlike I_A, lacked fast inactivation. Candidate channels include members of the K_V7 (KCNQ, M-current) family, which have been identified previously in rodent vestibular HCs (Kharkovets et al., 2000; Rennie et al., 2001; Hurley et al., 2006; Scheffer et al., 2015).

We test for K_V7 contributions in $K_V1.8^{-/-}$ type I HCs, $K_V1.8^{-/-}$ type II HCs, and $K_V1.8^{+/+,+/-}$ type II HCs of multiple ages by applying XE991 at 10 µM (Fig. 7A), a dose selective for K_V7 channels (Brown et al., 2002) and close to the IC_{50} (Alexander et al., 2019). In $K_V1.8^{-/-}$ HCs of both types, 10 µM XE991 blocked about half of the residual K_V conductance (Fig. 7B.1), consistent with K_V7 channels conducting most or all of the non-$K_V1.8$ delayed rectifier current. In all tested HCs (P8-355, median P224), the XE991-sensitive conductance did not inactivate substantially within 200 ms at any voltage, consistent with $K_V7.2$, 7.3, 7.4, and 7.5 currents (Wang, 1998; Kubisch et al., 1999; Schroeder et al., 2000; Jensen et al., 2007; Xu et al., 2007). We refer to this component as $g_{DR}(K_V7)$. The voltage dependence and Gmax density (G_{max}/C_m) of $g_{DR}(K_V7)$ were comparable across HC types and genotypes (Figure 7B.2-4).

These results are consistent with similar K_V7 channels contributing a relatively small delayed rectifier in both HC types. In addition, the similarity of XE991-sensitive currents of $K_V1.8^{+/+}$ and $K_V1.8^{-/-}$ type II HCs indicates that knocking out $K_V1.8$ did not cause general effects on ion channel expression. We did not test XE991 on $K_V1.8^{+/+,+/-}$ type I HCs because $g_{K,L}$ runs down in ruptured patch recordings (Rüsch and Eatock, 1996a; Chen and Eatock, 2000; Hurley et al., 2006), which could contaminate the XE991-sensitive conductance obtained by subtraction.

In one striolar $K_V1.8^{-/-}$ type I HC, XE991 also blocked a small conductance that activated negative to rest (Suppl. Fig. 5A-B). This conductance (V_{half} ~= –100 mV, Suppl. Fig. 5C) was detected only in $K_V1.8^{-/-}$ type I HCs from the striola (5/23 vs. 0/45 extrastriolar). The V_{half} and $\tau_{deactivation}$ at –124 mV were similar to values reported for $K_V7.4$ channels in cochlear HCs (Wong et al., 2004; Dierich et al., 2020). This very negatively activating K_V7 conductance coexisted with the larger less negatively activating K_V7 conductance (Suppl. Fig. 5C) and was too small (<0.5 nS/pF) to contribute significantly to $g_{K,L}$ (~10-100 nS/pF, Fig. 1D).

Other channels

While our data are consistent with $K_V1.8$- and K_V7- containing channels carrying most of the outward-rectifying current in mouse utricular hair cells, there is evidence in other preparations for additional channels, including K_V11 (KCNH, Erg) channels in rat utricular type I hair cells (Hurley et al., 2006) and BK (KCNMA1) channels in rat utricle and rat and turtle semicircular canal hair cells (Schweizer et al., 2009; Contini et al., 2020).

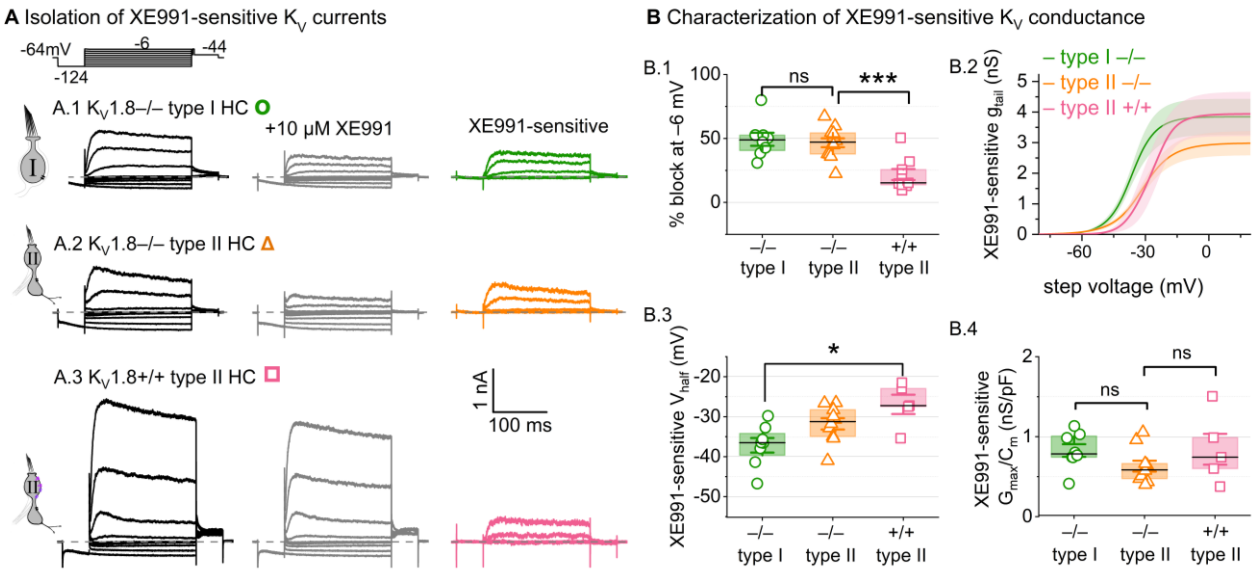

Figure 7. A K_V7-selective blocker, XE991, reduced residual delayed rectifier currents in $K_V1.8^{-/-}$ type I and II HCs.
(A) XE991 (10 µM) partly blocked similar delayed rectifier currents in type I and type II $K_V1.8^{-/-}$ HCs and a type II $K_V1.8^{+/+}$ HC.
(B) Properties of XE991-sensitive conductance, $g_{DR}(K_V7)$. (**B.1**) % Block of steady-state current. (**B.2**) tail G-V curves for $K_V1.8^{-/-}$ type I HCs (n=8), $K_V1.8^{-/-}$ type II HCs (9), and $K_V1.8^{+/+}$ type II HCs (5); mean ± SEM. (**B.3**) V_{half} was less negative in $K_V1.8^{+/+}$ type II than $K_V1.8^{-/-}$ type I HC (p = 0.01, KWA). (**B.4**) Conductance density was similar in all groups (ANOVA, non-significant at 40% power (*left*), 20% power (*right*).

BK is expressed in mouse utricular hair cells (McInturff et al., 2018; Jan et al., 2021; Orvis et al., 2021). However, Ca^{2+}-dependent currents have not been observed in mouse utricular HCs, and we found little to no effect of the BK-channel blocker iberiotoxin at a dose (100 nM) well beyond the IC_{50}: percent blocked at –30 mV was 2 ± 6% (3 $K_V1.8^{-/-}$ type I HCs); 1 ± 5% (5 $K_V1.8^{+/+,+/-}$ type II HCs); 7% and 14% (2 $K_V1.8^{-/-}$ type II HCs). We also did not see N-shaped I-V curves typical of many Ca^{2+}-dependent K^+ currents. In our ruptured-patch recordings, Ca^{2+}-dependent BK currents and erg channels may have been eliminated by wash-out of the hair cells' small Ca_V currents (Bao et al., 2003) or cytoplasmic second messengers (Hurley et al., 2006).

To check whether the constitutive $K_V1.8$ knockout has strong non-specific effects on channel trafficking, we examined the summed HCN and inward rectifier currents (I_H and I_{Kir}) at –124 mV, and found them similar across genotypes (Suppl. Fig. 6). In the process, we noted zonal differences in I_H and I_{Kir} that have not been reported in hair cells. In type I HCs from both control and null utricles, I_H and I_{Kir} were less prevalent in striola than extrastriola, and, when present, the combined inward current was smaller (Suppl. Fig. 6B).

Discussion

We have shown that constitutive knockout of $K_V1.8$ eliminated $g_{K,L}$ in type I HCs, and g_A and much of g_{DR} in type II HCs. $K_V1.8$ immunolocalized specifically to the basolateral membranes of type I and II HCs. We conclude that $K_V1.8$ is a pore-forming subunit of $g_{K,L}$, g_A, and part of g_{DR} [$g_{DR}(K_V1.8)$]. We provide evidence that fast inactivation of g_A may arise from heteromultimerization of non-inactivating $K_V1.8$ subunits and inactivating $K_V1.4$ subunits. Finally, we showed that a substantial component of the residual delayed rectifier current in both type I and type II HCs comprises K_V7 channels.

$K_V1.8$ is expressed in hair cells from mammalian cochlea (Dierich et al., 2020), avian utricle (Scheibinger et al., 2022), and zebrafish (Erickson and Nicolson, 2015). Our work suggests that in anamniotes, which lack type I cells and $g_{K,L}$, $K_V1.8$ contributes to g_A and g_{DR}, which are widespread in vertebrate HCs (reviewed in Meredith and Rennie, 2016). $K_V1.8$ expression has not been detected in rodent brain but is reported in the pacemaker nucleus of weakly electric fish (Smith et al., 2018).

$K_V1.8$ subunits may form homomultimers to produce $g_{K,L}$ in type I hair cells

Recent single-cell expression studies on mouse utricles (McInturff et al., 2018; Jan et al., 2021; Orvis et al., 2021) have detected just one K_V1 subunit, $K_V1.8$, in mouse type I HCs. Given that $K_V1.8$ can only form multimers with K_V1 family members, and given that $g_{K,L}$ channels are present at very high density (~150 per μm^2 in rat type I, Chen and Eatock, 2000), it stands to reason that most or all of the channels are $K_V1.8$ homomers. Other evidence is consistent with this proposal. $g_{K,L}$ (Rüsch and Eatock, 1996a) and heterologously expressed $K_V1.8$ homomers in oocytes (Lang et al., 2000) are non-inactivating and blocked by millimolar Ba^{2+} and 4-aminopyridine and >10 mM TEA. Unlike channels with $K_V1.1$, $K_V1.2$, and $K_V1.6$ subunits, $g_{K,L}$ is not sensitive to 10 nM α-dendrotoxin (Rüsch and Eatock, 1996a). $g_{K,L}$ and heterologously expressed $K_V1.8$ channels have similar single-channel conductances (~20 pS for $g_{K,L}$ at positive potentials, Chen and Eatock, 2000; 11 pS in oocytes, Lang et al., 2000). $g_{K,L}$ is inhibited—or positively voltage-shifted—by cGMP (Behrend et al., 1997; Chen and Eatock, 2000), presumably via the C-terminal cyclic nucleotide binding domain of $K_V1.8$.

A major novel property of $g_{K,L}$ is that it activates 30-60 mV negative to type II $K_V1.8$ conductances and most other low-voltage-activated K_V channels (Ranjan et al., 2019). The very negative activation range is a striking difference between $g_{K,L}$ and known homomeric $K_V1.8$ channels. Heterologously expressed homomeric $K_V1.8$ channels have an activation V_{half} of –10 to 0 mV (*X. laevis* oocytes, Lang et al., 2000; CHO cells, Dierich et al., 2020). In cochlear inner HCs, currents attributed to $K_V1.8$ (by subtraction of other candidates) have a near-zero activation V_{half} (–4 mV, Dierich et al., 2020).

Possible factors in the unusually negative voltage dependence of $g_{K,L}$ include:

1) elevation of extracellular K^+ by the enveloping calyceal terminal, unique to type I HCs (Lim et al., 2011; Contini et al., 2012; Spaiardi et al., 2020; Govindaraju et al., 2023). High K^+ increases conductance though $g_{K,L}$ channels (Contini et al., 2020), perhaps through K^+-mediated relief of C-type inactivation (López-Barneo et al., 1993; Baukrowitz and Yellen, 1995). We note, however, that $g_{K,L}$ is open at rest even in neonatal mouse utricles cultured without innervation (Rüsch et al., 1998) and persists in dissociated type I HCs (Chen and Eatock, 2000; Hurley et al., 2006).

2) The high density of $g_{K,L}$ (~50 nS/pF in striolar $K_V1.8^{+/+}$ HCs) implies close packing of channels, possibly represented by particles (12-14 nm) seen in freeze-fracture electron microscopy of the type I HC membrane (Gulley and Bagger-Sjöbäck, 1979; Sousa et al., 2009). Such close channel packing might

hyperpolarize *in situ* voltage dependence of $g_{K,L}$, as proposed for $K_V7.4$ channels in outer hair cells (Perez-Flores et al., 2020).

3) Modulation by accessory subunits. Type I HCs express $K_V\beta1$ (McInturff et al., 2018; Orvis et al., 2021), an accessory subunit that can confer fast inactivation and hyperpolarize activation V_{half} by ~10 mV. $K_V\beta1$ might interact with $K_V1.8$ to shift voltage dependence negatively. Arguments against this possibility include that $g_{K,L}$ lacks fast inactivation (Rüsch and Eatock, 1996a; Hurley et al., 2006; Spaiardi et al., 2017) and that cochlear inner hair cells co-express $K_V1.8$ and $K_V\beta1$ (Liu et al., 2018) but their $K_V1.8$ conductance has a near-0 V_{half} (Dierich et al., 2020).

$K_V1.8$ subunits may heteromerize with variable numbers of inactivating $K_V1.4$ subunits to produce g_A and $K_V1.8$-dependent g_{DR} in type II HCs

The $K_V1.8$-dependent conductances of type II HCs vary in their fast and slow inactivation. In not showing fast inactivation (Lang et al., 2000; Ranjan et al., 2019; Dierich et al., 2020), heterologously expressed $K_V1.8$ subunits resemble most other K_V1 family subunits, with the exception of $K_V1.4$ (for comprehensive review, see Ranjan et al., 2019). $K_V1.4$ is a good candidate to provide fast inactivation based on immunolocalization and voltage dependence (Figs. 4, 6). We suggest that g_A and $g_{DR}(K_V1.8)$ are $K_V1.8$-containing channels that vary in $K_V1.8$:$K_V1.4$ stoichiometry, with possible additional variation in $K_V\beta2$ and $K_V\beta1$ accessory subunits.

$K_V1.4$-$K_V1.8$ heteromeric assembly could account for several related observations. The faster $\tau_{Inact,Fast}$ in $K_V1.8^{+/-}$ relative to $K_V1.8^{+/+}$ type II HCs (Fig. 3A.3, Suppl. Fig. 2A.1) could reflect an increased ratio of $K_V1.4$ to $K_V1.8$ subunits and therefore more N-terminal inactivation domains per heteromeric channel. Zonal variation in the extent and speed of N-type inactivation (Fig. 3A) might arise from differential expression of $K_V1.4$. The small fast-inactivating conductance in ~20% of extrastriolar $K_V1.8^{-/-}$ type II HCs (Suppl. Fig. 4) might flow through $K_V1.4$ homomers.

In addition or alternatively, $K_V\beta$ subunits are positioned to contribute to fast inactivation. $K_V\beta1$ is expressed in type II HCs (McInturff et al., 2018; Jan et al., 2021; Orvis et al., 2021), and, together with $K_V1.4$, has been linked to g_A in pigeon vestibular HCs (Correia et al., 2008). $K_V\beta2$, also expressed in type II HCs (McInturff et al., 2018; Orvis et al., 2021), does not confer fast inactivation but hyperpolarizes activation voltage by ~10 mV and accelerates activation and inactivation kinetics (Heinemann et al., 1996).

g_A and $g_{DR}(K_V1.8)$ are not likely to be different kinetic components of current through homogeneous incompletely inactivating K_V channels. The lack of N-type inactivation of $g_{DR}(K_V1.8)$ is readily explained by homomeric $K_V1.8$ channels. The double-exponential decay of g_{Peak} (comprising g_A and $g_{DR}(K_V1.8)$) is consistent with two channel populations.

$K_V1.8$ relevance for vestibular function

In both type I and type II utricular HCs, $K_V1.8$-dependent channels strongly shape receptor potentials in ways that promote temporal fidelity rather than electrical tuning (Lewis, 1988), consistent with the utricle's role in driving reflexes that compensate for head motions as they occur. This effect is especially pronounced for type I HCs, where the current-step evoked voltage response reproduces the input with great speed and linearity (Fig. 2).

$g_{K,L}$ dominates passive membrane properties in mature $K_V1.8^{+/+,+/-}$ type I HCs such that $K_V1.8^{-/-}$ type I HCs are expected to have receptor potentials with higher amplitudes but lower low-pass corner frequencies, closer to those of type II HCs and immature HCs of all types (Correia et al., 1996; Rüsch and

414 Eatock, 1996a; Songer and Eatock, 2013). In $K_V1.8^{-/-}$ epithelia, we expect the lack of a large basolateral
415 conductance open at rest to reduce the speed and gain of non-quantal transmission, which depends on
416 K^+ ion efflux from the type I HC to change electrical and K^+ potentials in the synaptic cleft (Govindaraju et
417 al., 2023). In hair cells, K^+ enters the mechanosensitive channels of the hair bundle from the K^+-rich apical
418 endolymph and exits through basolateral potassium conductances into the more conventional low-K+
419 perilymph. For the type I-calyx synapse, having in the hair cell a large, non-inactivating K^+ conductance
420 open across the physiological range of potentials avoids channel gating time and allows for instantaneous
421 changes in current into the cleft and fast afferent signaling (Pastras et al., 2023).
422 In contrast, mature type II HCs face smaller synaptic contacts and have $K_V1.8$-dependent currents that
423 are not substantially activated at resting potential. They do affect the time course and gain of type II HC
424 responses to input currents, speeding up depolarizing transients, producing a repolarizing rebound during
425 the step, and reducing resonance.
426 Type I and II vestibular hair cells are closely related, such that adult type II HCs acquire type I-like
427 properties upon deletion of the transcription factor Sox2 (Stone et al., 2021). In normal development of
428 the two cell types, the Kcna10 gene generates importantly different ion channels, presenting a natural
429 experiment in functional differentiation of sensory receptor cells.
430
431
432

433 # Materials and methods

434 ## Preparation

435 All procedures for handling animals followed the NIH Guide for the Care and Use of Laboratory Animals
436 and were approved by the Institutional Animal Care and Use Committees of the University of Chicago and
437 the University of Illinois Chicago. Most mice belonged to a transgenic line with a knockout allele of *Kcna10*
438 (referred to here as $K_V1.8^{-/-}$). Our breeding colony was established with a generous gift of such animals
439 from Sherry M. Jones and Thomas Friedman. These animals are described in their paper (Lee et al., 2013).
440 Briefly, the Texas A&M Institute for Genomic Medicine generated the line on a C57BL/6;129SvEv mixed
441 background by replacing Exon 3 of the *Kcna10* gene with an IRES-bGeo/Purocassette. Mice in our colony
442 were raised on a 12:12h light-dark cycle with access to food and water *ad libitum*.
443 Semi-intact utricles were prepared from ~150 male and ~120 female mice, postnatal days (P) 5-375,
444 for same-day recording. Hair cell K_V channel data were pooled across sexes as most results did not appear
445 to differ by sex; an exception was that $g_{K,L}$ had a more negative V_{half} in males (Suppl. Table 1), an effect not
446 clearly related to age, copy number, or other properties of the activation curve.
447 Preparation, stimulation, and recording methods followed our previously described methods for the
448 mouse utricle (Vollrath and Eatock, 2003). Mice were anesthetized through isoflurane inhalation. After
449 decapitation, each hemisphere was bathed in ice-cold, oxygenated Liebowitz-15 (L15) media. The
450 temporal bone was removed, the labyrinth was cut to isolate the utricle, and the nerve was cut close to
451 the utricle. The utricle was treated with proteinase XXIV (100 μg/mL, ~10 mins, 22°C) to facilitate removal
452 of the otoconia and attached gel layer and mounted beneath two glass rods affixed at one end to a
453 coverslip.
454

Electrophysiology

For most recordings, we used the HEKA Multiclamp EPC10 with Patchmaster acquisition software, filtered by the integrated HEKA filters: a 6-pole Bessel filter at 10 kHz and a second 4-pole Bessel filter at 5 kHz, and sampled at 10-100 kHz. Recording electrodes were pulled (PC-100, Narishige) from soda lime glass (King's Precision Glass R-6) wrapped in paraffin to reduce pipette capacitance. Internal solution contained (in mM) 135 KCl, 0.5 $MgCl_2$, 3 MgATP, 5 HEPES, 5 EGTA, 0.1 $CaCl_2$, 0.1 Na-cAMP, 0.1 LiGTP, 5 $Na_2CreatinePO_4$ adjusted to pH 7.25 and ~280 mmol/kg by adding ~30 mM KOH. External solution was Liebowitz-15 media supplemented with 10 mM HEPES (pH 7.40, 310 ± 10 mmol/kg). Recording temperature was 22-25°C. Pipette capacitance and membrane capacitance transients were subtracted during recordings with Patchmaster software. Series resistance (8-12 MΩ) was measured after rupture and compensated 60-80% with the amplifier, to final values of ~2 MΩ. Potentials are corrected for remaining (uncompensated) series resistance and liquid junction potential of ~4 mV, calculated with LJPCalc software (Marino et al., 2014).

Type I HCs with $g_{K,L}$ were transiently hyperpolarized to –90 mV to close $g_{K,L}$ enough to increase R_{input} above 100 MΩ, as needed to estimate series resistance and cell capacitance. The average resting potential, V_{rest}, was –87 mV ± 1 (41), similar to the calculated E_K of –86.1 mV, which is not surprising given the large K^+ conductance of these cells (Fig. 1). V_{rest} is likely more positive *in vivo*, where lower endolymphatic Ca^{2+} increases standing inward current through MET channels.

Voltage protocols to characterize K_V currents differed slightly for type I and II HCs. In standard protocols, the cell is held at a voltage near resting potential (–74 mV in type I and –64 mV in type II), then jumped to –124 mV for 200 ms in type I HCs in order to fully deactivate $g_{K,L}$ and 50 ms in type II HCs in order to remove baseline inactivation of g_A. The subsequent iterated step depolarizations lasted 500 ms in type I HCs because $g_{K,L}$ activates slowly (Wong et al., 2004) and 200 ms in type II HCs, where K_V conductances activate faster. The 50-ms tail voltage was near the reversal potential of HCN channels (–44 mV in mouse utricular hair cells, Rüsch et al., 1998) to avoid HCN current contamination.

G-V (activation) parameters for control type I cells may be expected to vary across experiments on semi-intact (as here), organotypically cultured and denervated (Rüsch et al.,1998), or dissociated-cell preparations, reflecting variation in retention of the calyx (Discussion) and voltage step durations (Wong et al., 2004) which elevate K^+ concentration around the hair cell. Nevertheless, the values we obtained for type I and type II HCs resemble values recorded elsewhere, including experiments in which extra care was taken to avoid extracellular K^+ accumulation (Spaiardi et al., 2017, 2020). The effects of K^+ accumulation on $g_{K,L}$'s steady-state activation curves are small because the operating range is centered on E_K and can be characterized with relatively small currents (Fig. 1A).

Pharmacology

For most experiments, we locally perfused drug-containing solutions with BASI Bee Hive syringes at a final flow rate of 20 µL/min and a dead time of ~30 s. Global bath perfusion was paused during drug perfusion and recording, and only one cell was used per utricle. Aliquots of test agents in solution were prepared, stored at –20°C, and thawed and added to external solution on the recording day (see Key Resources Table).

Analysis

Data analysis was performed with software from OriginLab (Northampton, MA) and custom MATLAB scripts using MATLAB fitting algorithms.

Fitting voltage dependence and time course of conductances

G-V curves. Current was converted to conductance (G) by dividing by driving force ($V - E_K$; E_K calculated from solutions). For type I HCs, tail G-V curves were generated from current 1 ms after the end of the iterated voltage test step. For type II HCs, peak G-V curves were generated from peak current during the step and steady-state G-V curves were generated from current 1 ms before the end of a 200 ms step. Sigmoidal voltage dependence of G-V curves was fit with the first-order Boltzmann equation (Eq. 1).

$$G(V) = G_{min} + \frac{G_{max}}{1 + e^{\frac{V_{half} - V}{S}}} \qquad (1)$$

V_{half} is the midpoint and S is the slope factor, inversely related to curve steepness near activation threshold.

Activation time course of type II HCs. For type II HCs lacking fast inactivation, outward current activation was fit with Eq. 2.

$$I(t) = I_{SS} * \left(1 - e^{-\frac{t}{\tau_w}}\right)^n + I_0 \qquad (2)$$

I_{SS} is steady-state current, τ_w is activation time constant, n is the state factor related to the number of closed states (typically constrained to 3), and I_o is baseline current.

To measure activation and inactivation time course of g_A, we used Eq. 3 to fit outward K^+ currents evoked by steps from –125 mV to above –50 mV (Rothman and Manis, 2003b).

$$I(t) = I_{max} * \left(1 - e^{-\frac{t}{\tau_w}}\right)^n * (1 - Z * (f * \left(1 - e^{-\frac{t}{\tau_{zf}}}\right) + (1 - f) * \left(1 - e^{-\frac{t}{\tau_{zs}}}\right)) + I_0 \qquad (3)$$

Z is total steady-state inactivation ($0 \leq Z < 1$ means incomplete inactivation, which allows the equation to fit non-inactivating delayed rectifier currents), f is the fraction of fast inactivation relative to total inactivation, I_{max} is maximal current, τ_{zf} and τ_{zs} are the fast and slow inactivation time constants. We chose to compare fit parameters at 30 ± 2 mV (91), where fast and slow inactivation were consistently separable and g_A was maximized. In most $K_V1.8^{-/-}$ and some striolar $K_V1.8^{+/+,+/-}$ cells, where fast inactivation was absent and adjusted R^2 did not improve on a single-exponential fit by >0.01, we constrained f in Eq. 3 to 0 to avoid overfitting.

For *Peak* G-V relations, peak conductance was taken from fitted curves (Eqs. 2 and 3). To construct '*Steady-state'* G-V relations, we used current at 200 ms (6 ± 1 % (94) greater than steady-state estimated from fits to Eq. 3 (Fig. 3C-D)).

Percent inactivation was calculated at 30 mV with Eq. 4 :

$$\%\, Inactivation = (I_{Peak} - I_{SS})/I_{Peak} \qquad (4)$$

I_{Peak} is maximal current, and I_{SS} is current at the end of a 200 ms voltage step.

The electrical resonance of type II HCs was quantified by fitting voltage responses to current injection steps (Songer and Eatock, 2013). We fit Eq. 5, a damped sinusoid, to the voltage trace from half-maximum of the initial depolarizing peak until the end of the current step.

$$V(t) = V_{ss} + V_p * e^{-\frac{t}{\tau_e}} * \sin(2\pi f_e - \theta) \quad (5)$$

V_{SS} is steady-state voltage, V_p is the voltage of the peak response, τ_e is the decay time constant, f_e is the fundamental frequency, and θ is the phase angle shift.

Quality factor, Q_e, was calculated with Eq. 6 (Crawford and Fettiplace, 1981).

$$Q_e = [(\pi f_e \tau_e)^2 + 0.25]^{1/2} \quad (6)$$

Statistics

We give means ± SEM for normally-distributed data, and otherwise, median and range. Data normality was assessed with the Shapiro-Wilk test for n<50 and the Kolmogorov-Smirnov test for n>50. To assess homogeneity of variance we used Levene's test. With homogeneous variance, we used two-way ANOVA for genotype and zone with the posthoc Tukey's test. When variance was non-homogeneous, we used one-way Welch ANOVA with the posthoc Games-Howell test. For data that were not normally distributed, we used the non-parametric one-way Kruskal-Wallis ANOVA (KWA) with posthoc Dunn's test. Effect size is Hedge's g (g). For age dependence, we used partial correlation coefficients controlling for genotype and zone. Statistical groups may have different median ages, but all have overlapping age ranges. In figures, asterisks represent p-value ranges as follows: *, p<0.05; **, p<0.01; ***, p<0.001; ****, p<0.0001.

Immunohistochemistry

Mice were anesthetized with Nembutal (80 mg/kg), then perfused transcardially with 40mL of physiological saline containing heparin (400 IU), followed by 2 mL/g body weight fixative (4% paraformaldehyde, 1% picric acid, and 5% sucrose in 0.1 M phosphate buffer at pH 7.4, sometimes with 1% acrolein). Vestibular epithelia were dissected in phosphate buffer, and tissues were cryoprotected in 30% sucrose-phosphate buffer overnight at 4°C. Otoconia were dissolved with Cal-Ex (Fisher Scientific) for 10 min. Frozen sections (35 µm) were cut with a sliding microtome. Immunohistochemistry was performed on free-floating sections. Tissues were first permeabilized with 4% Triton X-100 in PBS for 1 h at room temperature, then incubated with 0.5% Triton X-100 in a blocking solution of 0.5% fish gelatin and 1% BSA for 1 h at room temperature. Sections were incubated with 2-3 primary antibodies for 72 h at 4°C and with 2-3 secondary antibodies. Sections were rinsed with PBS between and after incubations and mounted on slides in Mowiol (Calbiochem).

Table 6. Key Resources Table

Antibody	Source	Catalog Number	Lot Number	Dilution
Rabbit anti-K_V1.8	Alomone	APC-157	0102	1:200 or 1:400
Mouse anti-K_V1.4	NeuroMab	P15385	5HK-05	1:400

Mouse IGg2a-conjugated anti-Tuj1	Covance	MMS-435P	B205808	1:300
Goat anti-calretinin	Millipore	AB1550	9669	1:600
Mouse IgG1-conjugated anti-K_V7.4	NeuroMab	2HK-65		1:200
Donkey anti-Rabbit Secondary Antibody, Alexa Fluor 594	Invitrogen	A21207	8652	1:200
Donkey anti-Goat 488 nm	Invitrogen	A21125	1920483	1:200
Goat anti-Mouse IgG1 594	Invitrogen	A11055	1869589	1:200
Chemicals and Peptides	Source	Catalog Number	Diluent	
Iberiotoxin	Alomone	STI-400	Water	
XE991 dihydrochloride	Sigma	X2254	Water	
ZD7288	Tocris	APN18035-2	Water	
Bovine serum albumin	Fisher	BP671	water	

Data Availability

Data used in this study are available on Dryad (https://doi.org/10.5061/dryad.37pvmcvrw).

Acknowledgements

This study was supported by NIH grant R01 DC012347 to RAE and AL and an NSF Graduate Research Fellowship to HRM. We thank Drs. Thomas Friedman and Sherri Jones for the generous gift of the $K_V1.8^{-/-}$ mouse line, and Drs. Zheng-Yi Chen and Deborah I. Scheffer for bringing the expression of this subunit in mouse vestibular hair cells to our attention.

We acknowledge Dr. Vicente Lumbreras for insights from his prior experiments on g_A in mouse utricular hair cells, and thank him for helpful further discussions.

We thank Drs. Rebecca Lim and Ebenezer Yamoah for their critical feedback on the manuscript, and Drs. Rob Raphael and Aravind Chenrayan Govindaraju for feedback and many helpful discussions. We thank Drs. Joe Burns, Gabi Pregernig, and Lars Becker (Decibel Therapeutics, Inc.) for helpful discussions.

Author Contributions

HRM designed and performed experiments, analyzed data, and wrote the paper; RAE helped design experiments, analyze data, and write the paper; AL performed immunohistochemistry experiments.

References

Alexander SPH et al. (2019) The Concise Guide to Pharmacology 2019/20: Ion channels. Br J Pharmacol 176 Available at: https://onlinelibrary.wiley.com/doi/10.1111/bph.14749 [Accessed April 12, 2022].

590 Al-Sabi A, Kaza S, Le Berre M, O'Hara L, Bodeker M, Wang J, Dolly JO (2011) Position-dependent
591 attenuation by Kv1.6 of N-type inactivation of Kv1.4-containing channels. Biochem J 438:389–
592 396.

593 Ashmore JF (1983) Frequency tuning in a frog vestibular organ. Nature 304:536–538.

594 Bao H, Wong WH, Goldberg JM, Eatock RA (2003) Voltage-Gated Calcium Channel Currents in Type I and
595 Type II Hair Cells Isolated From the Rat Crista. J Neurophysiol 90:155–164.

596 Baukrowitz T, Yellen G (1995) Modulation of K+ current by frequency and external [K+]: A tale of two
597 inactivation mechanisms. Neuron 15:951–960.

598 Behrend O, Schwark C, Kunihiro T, Strupp M (1997) Cyclic GMP inhibits and shifts the activation curve of
599 the delayed rectifier (I(K1)) of type I mammalian vestibular hair cells. NeuroReport 8:2687–2690.

600 Brown DA, Selyanko AA, Hadley JK, Tatulian L (2002) Some Pharmacological Properties Of Neural KCNQ
601 Channels. Neurophysiology 34:91–94.

602 Carlisle FA, Steel KP, Lewis MA (2012) Specific expression of Kcna10, Pxn and Odf2 in the organ of Corti.
603 Gene Expression Patterns 12:172–179.

604 Chen JWY, Eatock RA (2000) Major Potassium Conductance in Type I Hair Cells from Rat Semicircular
605 Canals: Characterization and Modulation by Nitric Oxide. J Neurophysiol 84:139–151.

606 Contini D, Holstein GR, Art JJ (2020) Synaptic cleft microenvironment influences potassium permeation
607 and synaptic transmission in hair cells surrounded by calyx afferents in the turtle. J Physiol
608 598:853–889.

609 Contini D, Price SD, Art JJ (2017) Accumulation of K^+ in the synaptic cleft modulates activity by
610 influencing both vestibular hair cell and calyx afferent in the turtle: K^+ modulation of synaptic
611 transmission between hair cell and afferent. J Physiol 595:777–803.

612 Contini D, Zampini V, Tavazzani E, Magistretti J, Russo G, Prigioni I, Masetto S (2012) Intercellular K^+
613 accumulation depolarizes Type I vestibular hair cells and their associated afferent nerve calyx.
614 Neuroscience 227:232–246.

615 Correia MJ, Lang DG (1990) An electrophysiological comparison of solitary type I and type II vestibular
616 hair cells. Neuroscience Letters 116:106–111.

617 Correia MJ, Ricci AJ, Rennie KJ (1996) Filtering Properties of Vestibular Hair Cells: An Update. Ann NY
618 Acad Sci 781:138–149.

619 Correia MJ, Weng T, Prusak D, Wood TG (2008) Kvβ1.1 Associates with Kv1.4 in Chinese Hamster Ovary
620 Cells and Pigeon Type II Vestibular Hair Cells and Enhances the Amplitude, Inactivation and
621 Negatively Shifts the Steady-State Inactivation Range. Neuroscience 152:809–820.

622 Crawford AC, Fettiplace R (1981) An electrical tuning mechanism in turtle cochlear hair cells. J Physiol
623 312:377–412.

624 Desai SS, Zeh C, Lysakowski A (2005) Comparative Morphology of Rodent Vestibular Periphery. I.
625 Saccular and Utricular Maculae. J Neurophysiol 93:251–266.

626 Dierich M, Altoè A, Koppelmann J, Evers S, Renigunta V, Schäfer MK, Naumann R, Verhulst S, Oliver D,
627 Leitner MG (2020) Optimized Tuning of Auditory Inner Hair Cells to Encode Complex Sound
628 through Synergistic Activity of Six Independent K+ Current Entities. Cell Reports 32:107869.

629 Dwenger MM, Raph SM, Baba SP, Moore JB, Nystoriak MA (2022) Diversification of Potassium Currents
630 in Excitable Cells via Kvβ Proteins. Cells 11:2230.

631 Eatock RA, Songer JE (2011) Vestibular Hair Cells and Afferents: Two Channels for Head Motion Signals.
632 Annu Rev Neurosci 34:501–534.

633 Erickson T, Nicolson T (2015) Identification of sensory hair-cell transcripts by thiouracil-tagging in
634 zebrafish. BMC Genomics 16:842.

635 Fettiplace R (1987) Electrical tuning of hair cells in the inner ear. TINS 10:5.

636 Géléoc GS, Risner J, Holt JR (2004) Developmental Acquisition of Voltage-Dependent Conductances and
637 Sensory Signaling in Hair Cells of the Embryonic Mouse Inner Ear. J Neurosci 24:11148–11159.

638 Goldberg JM (2000) Afferent diversity and the organization of central vestibular pathways. Exp Brain Res
639 130:277–297.

640 González-Garrido A, Pujol R, López-Ramírez O, Finkbeiner C, Eatock RA, Stone JS (2021) The
641 Differentiation Status of Hair Cells That Regenerate Naturally in the Vestibular Inner Ear of the
642 Adult Mouse. J Neurosci 41:7779–7796.

643 Govindaraju AC, Quraishi IH, Lysakowski A, Eatock RA, Raphael RM (2023) Nonquantal transmission at
644 the vestibular hair cell–calyx synapse: K_{LV} currents modulate fast electrical and slow K^+
645 potentials. Proc Natl Acad Sci USA 120:e2207466120.

646 Gulley A, Bagger-Sjöbäck D (1979) Freeze-fracture studies on the synapse between the type I hair cells
647 and the calyceal terminal in the guinea-pig vestibular system. J Neurocytol 8:591–603.

648 Heinemann SH, Rettig J, Graack HR, Pongs O (1996) Functional characterization of Kv channel beta-
649 subunits from rat brain. J Physiol 493:625–633.

650 Holt JR, Stauffer EA, Abraham D, Geleoc GSG (2007) Dominant-Negative Inhibition of M-Like Potassium
651 Conductances in Hair Cells of the Mouse Inner Ear. J Neurosci 27:8940–8951.

652 Hudspeth AJ, Lewis RS (1988) A model for electrical resonance and frequency tuning in saccular hair cells
653 of the bull-frog, Rana catesbeiana. J Physiol 400:275–297.

654 Hurley KM, Gaboyard S, Zhong M, Price SD, Wooltorton JRA, Lysakowski A, Eatock RA (2006) M-Like K^+
655 Currents in Type I Hair Cells and Calyx Afferent Endings of the Developing Rat Utricle. Journal of
656 Neuroscience 26:10253–10269.

657 Imbrici P, D'Adamo MC, Kullmann DM, Pessia M (2006) Episodic ataxia type 1 mutations in the *KCNA1*
658 gene impair the fast inactivation properties of the human potassium channels Kv1.4-1.1/Kvβ1.1
659 and Kv1.4-1.1/Kvβ1.2. Eur J Neurosci 24:3073–3083.

660 Jan TA, Eltawil Y, Ling AH, Chen L, Ellwanger DC, Heller S, Cheng AG (2021) Spatiotemporal dynamics of
661 inner ear sensory and non-sensory cells revealed by single-cell transcriptomics. Cell Reports
662 36:109358.

663 Jensen HS, Grunnet M, Olesen S-P (2007) Inactivation as a New Regulatory Mechanism for Neuronal Kv7
664 Channels. Biophys J 92:2747–2756.

665 Kharkovets T, Hardelin J-P, Safieddine S, Schweizer M, El-Amraoui A, Petit C, Jentsch TJ (2000) KCNQ4, a
666 K^+ channel mutated in a form of dominant deafness, is expressed in the inner ear and the central
667 auditory pathway. Proc Natl Acad Sci USA 97:4333–4338.

668 Kubisch C, Schroeder BC, Friedrich T, Lütjohann B, El-Amraoui A, Marlin S, Petit C, Jentsch TJ (1999)
669 KCNQ4, a Novel Potassium Channel Expressed in Sensory Outer Hair Cells, Is Mutated in
670 Dominant Deafness. Cell 96:437–446.

671 Lang R, Lee G, Liu W, Tian S, Rafi H, Orias M, Segal AS, Desir GV (2000) KCNA10: A novel ion channel
672 functionally related to both voltage-gated potassium and CNG cation channels. American
673 Journal of Physiology - Renal Physiology 278.

674 Lee SI, Conrad T, Jones SM, Lagziel A, Starost MF, Belyantseva IA, Friedman TB, Morell RJ (2013) A null
675 mutation of mouse Kcna10 causes significant vestibular and mild hearing dysfunction. Hear Res
676 300:1–9.

677 Lewis ER (1988) Tuning in the bullfrog ear. Biophysical Journal 53:441–447.

678 Liberman MC, Gao J, He DZZ, Wu X, Jia S, Zuo J (2002) Prestin is required for electromotility of the outer
679 hair cell and for the cochlear amplifier. Nature 419:300–304.

680 Lim R, Kindig AE, Donne SW, Callister RJ, Brichta AM (2011) Potassium accumulation between type I hair
681 cells and calyx terminals in mouse crista. Exp Brain Res 210:607–621.

682 Liu H, Chen L, Giffen KP, Stringham ST, Li Y, Judge PD, Beisel KW, He DZZ (2018) Cell-Specific
683 Transcriptome Analysis Shows That Adult Pillar and Deiters' Cells Express Genes Encoding
684 Machinery for Specializations of Cochlear Hair Cells. Front Mol Neurosci 11:356.

685 López-Barneo J, Hoshi T, Heinemann SH, Aldrich RW (1993) Effects of external cations and mutations in
686 the pore region on C-type inactivation of Shaker potassium channels. Recept Channels 1:61–71.

687 Lysakowski A, Gaboyard-Niay S, Calin-Jageman I, Chatlani S, Price SD, Eatock RA (2011) Molecular
688 Microdomains in a Sensory Terminal, the Vestibular Calyx Ending. J Neurosci 31:10101–10114.

689 Lysakowski A, Goldberg JM (2004) Morphophysiology of the vestibular periphery. In: The Vestibular
690 System, pp 57–152 Springer Hearing and Auditory Research. Springer New York. Available at:
691 https://doi.org/10.1007/0-387-21567-0_3.

692 Marino M, Misuri L, Brogioli D (2014) A new open source software for the calculation of the liquid
693 junction potential between two solutions according to the stationary Nernst-Planck equation.
694 Available at: http://arxiv.org/abs/1403.3640 [Accessed October 23, 2023].

695 McInturff S, Burns JC, Kelley MW (2018) Characterization of spatial and temporal development of Type I
696 and Type II hair cells in the mouse utricle using new cell-type-specific markers. Biol Open
697 7:bio038083.

698 Meredith FL, Rennie KJ (2016) Channeling your inner ear potassium: K+ channels in vestibular hair cells.
699 Hear Res 338:40–51.

700 Orvis J et al. (2021) gEAR: Gene Expression Analysis Resource portal for community-driven, multi-omic
701 data exploration. Nat Methods 18:843–844.

702 Pastras CJ, Curthoys IS, Asadnia M, McAlpine D, Rabbitt RD, Brown DJ (2023) Evidence that ultrafast non-
703 quantal transmission underlies synchronized vestibular action potential generation. J
704 Neurosci:JN-RM-1417-23.

705 Perez-Flores MC, Lee JH, Park S, Zhang X-D, Sihn C-R, Ledford HA, Wang W, Kim HJ, Timofeyev V, Yarov-
706 Yarovoy V, Chiamvimonvat N, Rabbitt RD, Yamoah EN (2020) Cooperativity of K_v 7.4 channels
707 confers ultrafast electromechanical sensitivity and emergent properties in cochlear outer hair
708 cells. Sci Adv 6:eaba1104.

709 Pujol R, Pickett SB, Nguyen TB, Stone JS (2014) Large basolateral processes on type II hair cells are novel
710 processing units in mammalian vestibular organs: Basolateral Processes of Type II Hair Cells. J
711 Comp Neurol 522:3141–3159.

712 Ramanathan K, Fuchs PA (2002) Modeling Hair Cell Tuning by Expression Gradients of Potassium
713 Channel. Biophys J 82:64–72.

714 Ranjan R, Logette E, Marani M, Herzog M, Tache V, Scantamburlo E, Buchilier V, Markram H (2019) A
715 Kinetic Map of the Homomeric Voltage-Gated Potassium Channel (Kv) Family. Front Cell
716 Neurosci 13:358.

717 Rennie KJ, Correia MJ (1994) Potassium currents in mammalian and avian isolated type I semicircular
718 canal hair cells. J Neurophysiol 71:317–329.

719 Rennie KJ, Weng T, Correia MJ (2001) Effects of KCNQ channel blockers on K^+ currents in vestibular hair
720 cells. Am J Physiol Cell Physiol 280:C473–C480.

721 Ricci AJ, Rennie KJ, Correia MJ (1996) The delayed rectifier, IKI, is the major conductance in type I
722 vestibular hair cells across vestibular end organs. Pflüg Arch Eur J Physiol 432:34–42.

723 Rothman JS, Manis PB (2003) Kinetic Analyses of Three Distinct Potassium Conductances in Ventral
724 Cochlear Nucleus Neurons. J Neurophysiol 89:3083–3096.

725 Rüsch A, Eatock RA (1996a) A delayed rectifier conductance in type I hair cells of the mouse utricle. J
726 Neurophysiol 76:995–1004.

727 Rüsch A, Eatock RA (1996b) Voltage Responses of Mouse Utricular Hair Cells to Injected Currents. Ann
728 NY Acad Sci 781:71–84.

729 Rüsch A, Lysakowski A, Eatock RA (1998) Postnatal development of type I and type II hair cells in the
730 mouse utricle: Acquisition of voltage-gated conductances and differentiated morphology.
731 Journal of Neuroscience 18:7487–7501.

732 Scheffer DI, Shen J, Corey DP, Chen Z-Y (2015) Gene Expression by Mouse Inner Ear Hair Cells during
733 Development. J Neurosci 35:6366–6380.

734 Scheibinger M, Janesick A, Benkafadar N, Ellwanger DC, Jan TA, Heller S (2022) Cell-type identity of the
735 avian utricle. Cell Reports 40:111432.

736 Schroeder BC, Hechenberger M, Weinreich F, Kubisch C, Jentsch TJ (2000) KCNQ5, a Novel Potassium
737 Channel Broadly Expressed in Brain, Mediates M-type Currents. Journal of Biological Chemistry
738 275:24089–24095.

739 Schweizer FE, Savin D, Luu C, Sultemeier DR, Hoffman LF (2009) Distribution of high-conductance
740 calcium-activated potassium channels in rat vestibular epithelia. J Comp Neurol 517:134–145.

741 Smith GT, Proffitt MR, Smith AR, Rusch DB (2018) Genes linked to species diversity in a sexually
742 dimorphic communication signal in electric fish. J Comp Physiol A 204:93–112.

743 Songer JE, Eatock RA (2013) Tuning and Timing in Mammalian Type I Hair Cells and Calyceal Synapses. J
744 Neurosci 33:3706–3724.

745 Sousa AD, Andrade LR, Salles FT, Pillai AM, Buttermore ED, Bhat MA, Kachar B (2009) The Septate
746 Junction Protein Caspr Is Required for Structural Support and Retention of KCNQ4 at Calyceal
747 Synapses of Vestibular Hair Cells. J Neurosci 29:3103–3108.

748 Spaiardi P, Tavazzani E, Manca M, Milesi V, Russo G, Prigioni I, Marcotti W, Magistretti J, Masetto S
749 (2017) An allosteric gating model recapitulates the biophysical properties of $I_{K,L}$ expressed in
750 mouse vestibular type I hair cells: Allosteric gating of $I_{K,L}$. J Physiol 595:6735–6750.

751 Spaiardi P, Tavazzani E, Manca M, Russo G, Prigioni I, Biella G, Giunta R, Johnson SL, Marcotti W,
752 Masetto S (2020) K+ Accumulation and Clearance in the Calyx Synaptic Cleft of Type I Mouse
753 Vestibular Hair Cells. Neuroscience 426:69–86.

754 Spitzmaul G, Tolosa L, Winkelman BHJ, Heidenreich M, Frens MA, Chabbert C, de Zeeuw CI, Jentsch TJ
755 (2013) Vestibular Role of KCNQ4 and KCNQ5 K+ Channels Revealed by Mouse Models*. Journal
756 of Biological Chemistry 288:9334–9344.

757 Stone JS, Pujol R, Nguyen TB, Cox BC (2021) The Transcription Factor Sox2 Is Required to Maintain the
758 Cell Type-Specific Properties and Innervation of Type II Vestibular Hair Cells in Adult Mice. J
759 Neurosci 41:6217–6233.

760 Stühmer W, Ruppersberg JP, Schröter KH, Sakmann B, Stocker M, Giese KP, Perschke A, Baumann A,
761 Pongs O (1989) Molecular basis of functional diversity of voltage-gated potassium channels in
762 mammalian brain. EMBO J 8:3235–3244.

763 Takahashi S, Sun W, Zhou Y, Homma K, Kachar B, Cheatham MA, Zheng J (2018) Prestin Contributes to
764 Membrane Compartmentalization and Is Required for Normal Innervation of Outer Hair Cells.
765 Front Cell Neurosci 12:211.

766 Vollrath MA, Eatock RA (2003) Time course and extent of mechanotransducer adaptation in mouse
767 utricular hair cells: Comparison with frog saccular hair cells. Journal of Neurophysiology
768 90:2676–2689.

769 Wang H (1998) KCNQ2 and KCNQ3 Potassium Channel Subunits: Molecular Correlates of the M-Channel.
770 Science 282:1890–1893.

771 Wersäll J (1956) Studies on the structure and innervation of the sensory epithelium of the cristae
772 ampulares in the guinea pig; a light and electron microscopic investigation. Acta Otolaryngol
773 Suppl 126:1–85.

774 Wong WH, Hurley KM, Eatock RA (2004) Differences Between the Negatively Activating Potassium
775 Conductances of Mammalian Cochlear and Vestibular Hair Cells. J Assoc Res Otolaryngol 5:270–
776 284.

777 Xu T, Nie L, Zhang Y, Mo J, Feng W, Wei D, Petrov E, Calisto LE, Kachar B, Beisel KW, Vazquez AE, Yamoah
778 EN (2007) Roles of Alternative Splicing in the Functional Properties of Inner Ear-specific KCNQ4
779 Channels. J Biol Chem 282:23899–23909.

780 Yao X (2002) Expression of KCNA10, a Voltage-Gated K Channel, in Glomerular Endothelium and at the
781 Apical Membrane of the Renal Proximal Tubule. Journal of the American Society of Nephrology
782 13:2831–2839.

783

784

785 ## Supplemental Figures

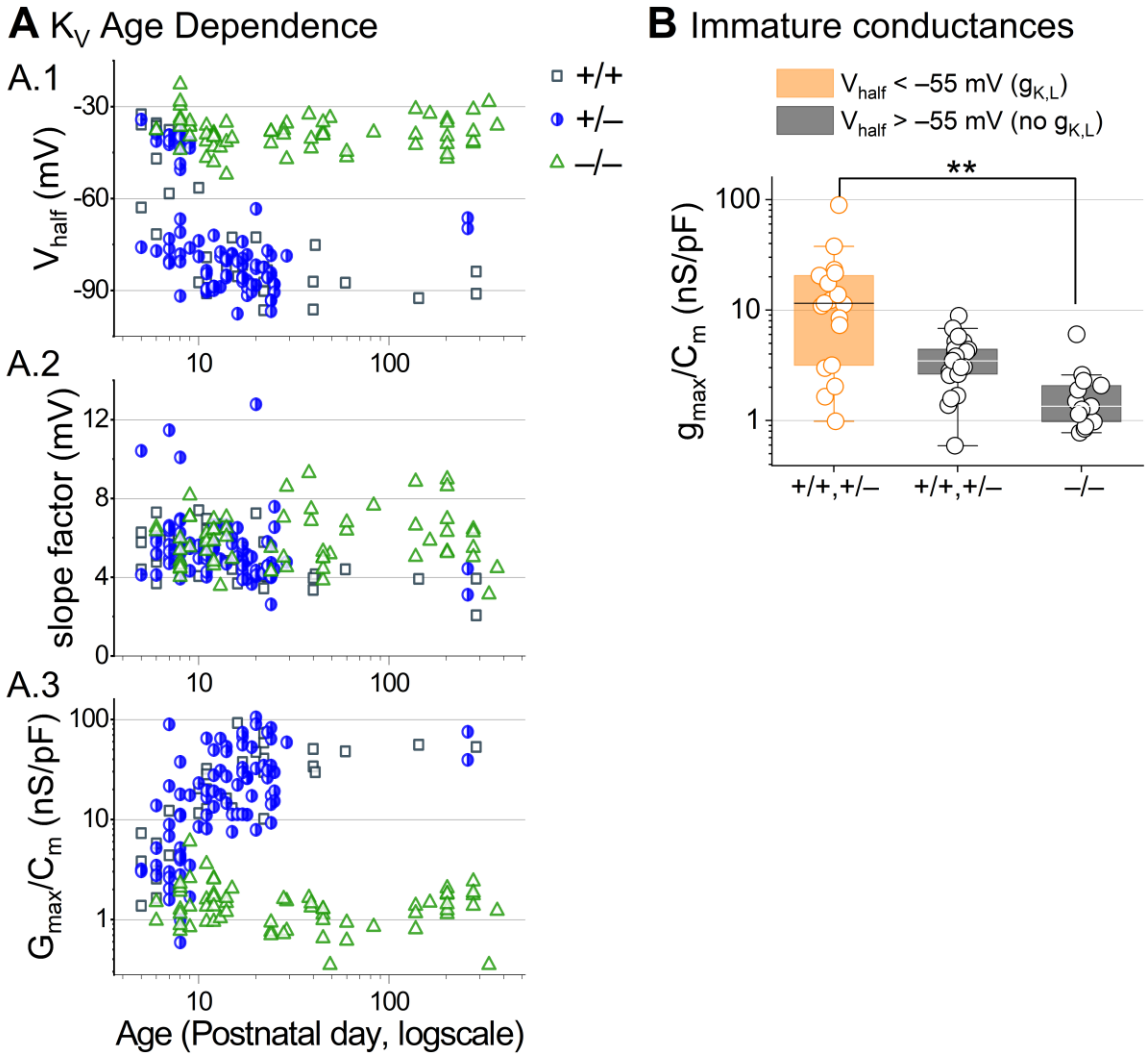

Supplemental Figure 1. Developmental changes in type I HC K_V conductances.
(**A**) Parameters from Boltzmann fits of tail G-V relations for type I HCs plotted against age.
(**B**) Conductance density is similar in young (P5-P10) type I HCs that lack $g_{K,L}$. $g_{K,L}$ is defined here as having a V_{half} negative to –55 mV. $K_V1.8^{+/+,+/-}$ *with* $g_{K,L}$, 17 ± 5 nS/pF (19); $K_V1.8^{+/+,+/-}$ *without* $g_{K,L}$, 3.7 ± 0.4 nS/pF (22); $K_V1.8^{-/-}$, 1.8 ± 0.4 nS/pF (13). $K_V1.8^{+/+,+/-}$ *with* $g_{K,L}$ vs. $K_V1.8^{-/-}$: p = 0.007, KWA, g 1.0.

786
787
788

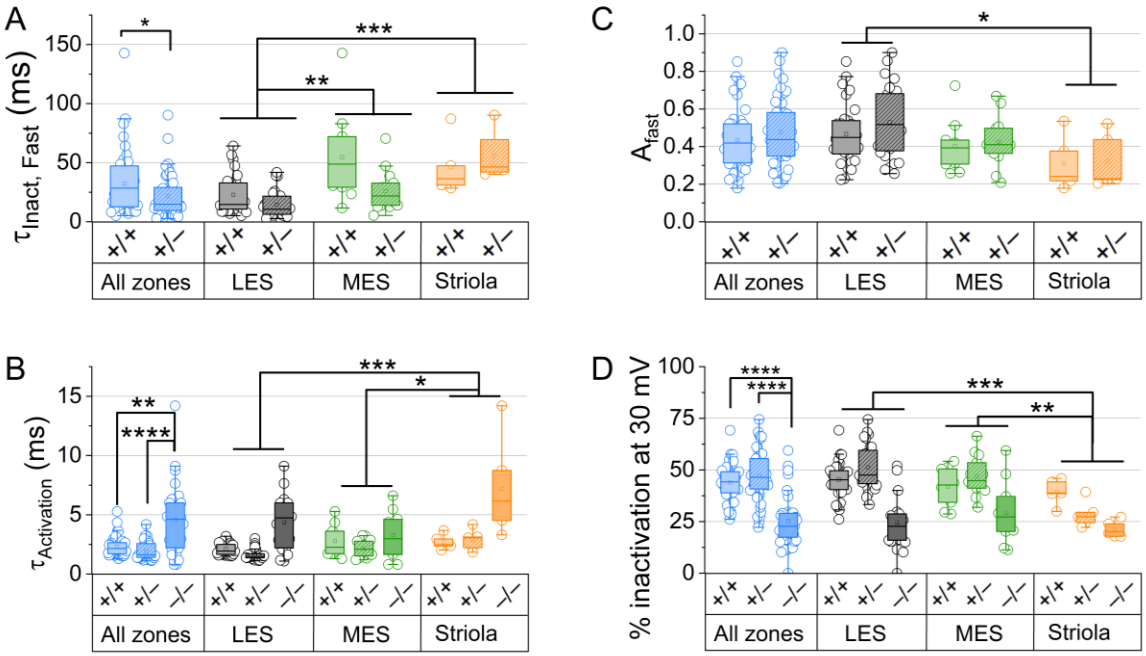

Supplemental Figure 2. **For type II HCs older than P12, K_V conductance activation and inactivation differed across zones and genotypes.**

(**A**) $\tau_{inact,Fast}$ at 30 mV was fastest in LES in $K_V1.8^{+/+}$ and $K_V1.8^{+/-}$ HCs, and faster in $K_V1.8^{+/-}$ than $K_V1.8^{+/+}$ HCs (see Table 3 for p-values).

(**B**) Fast inactivation was a larger fraction of the total in LES than striola.

(**C**) τ_{Act} at 30 mV was slower in $K_V1.8^{-/-}$ than $K_V1.8^{+/+}$ and $K_V1.8^{+/-}$, and slower in striola than LES and MES.

(**D**) Percent inactivation at 30 mV was lowest in striola (zone effect), and lowest in $K_V1.8^{-/-}$ HCs (genotype effect).

789

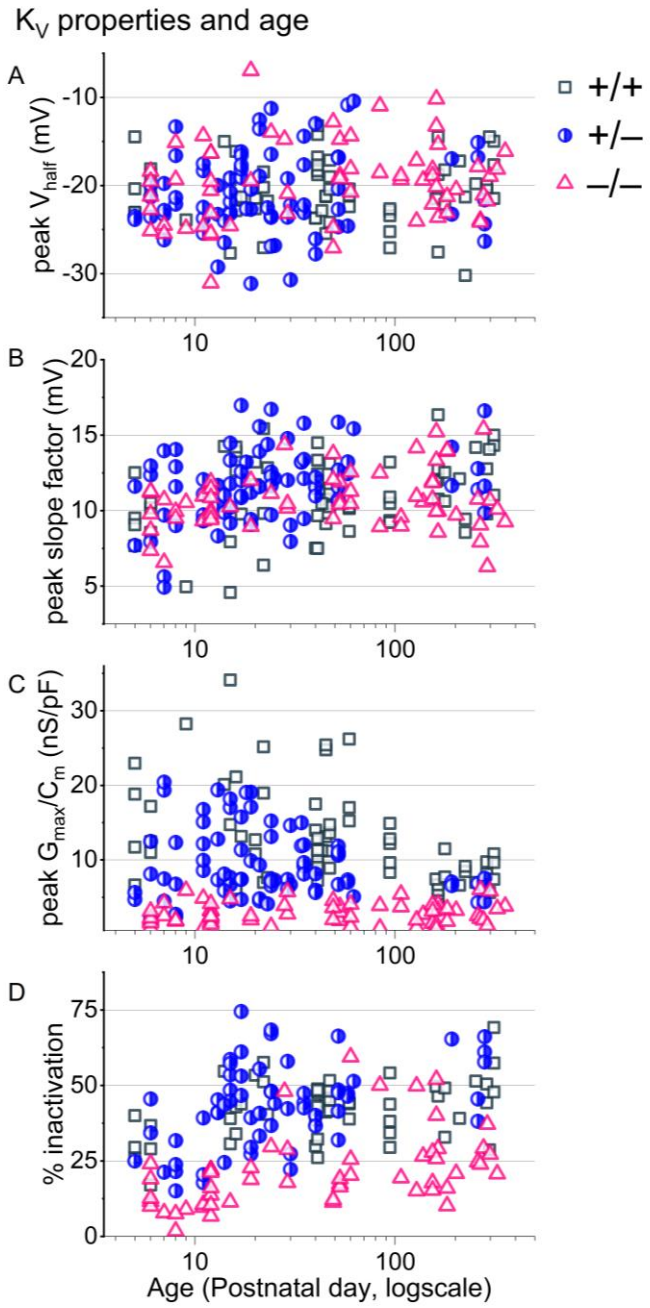

Supplemental Figure 3. For type II HCs older than P12, K_V conductances were stable.
(**A-C**) Parameters from Boltzmann fits of peak G-V relations and (**D**) % inactivation at +30 mV plotted against age from all zones. Overlaid curves are smoothing cubic β-splines. Note the seven extrastriolar $K_V1.8^{-/-}$ type II HCs with % inactivation >30%.

790
791
792
793

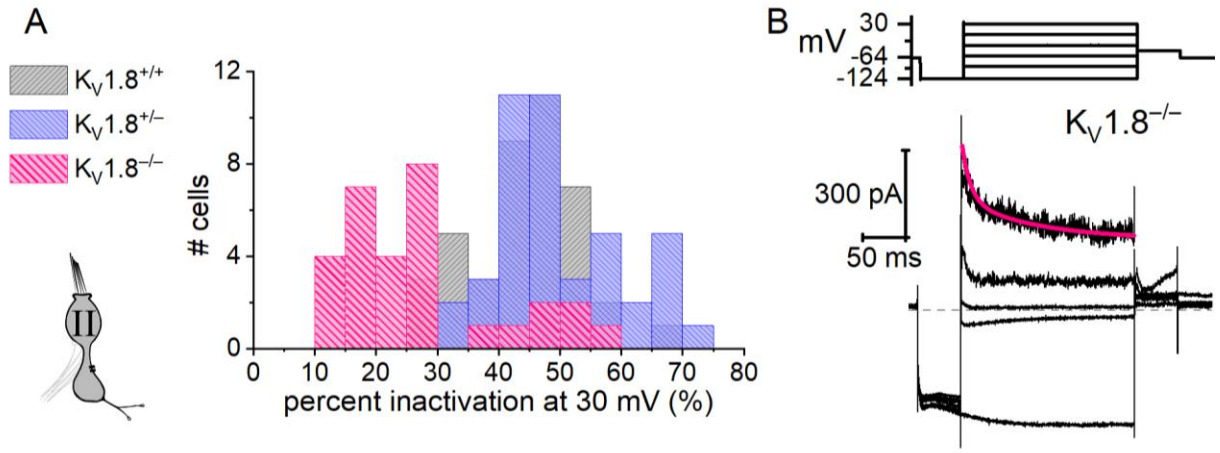

Supplemental Figure 4. A minority of extrastriolar $K_V1.8^{-/-}$ type II HCs had a very small fast-inactivating outward rectifier current.

(**A**) All extrastriolar $K_V1.8^{+/+,+/-}$ type II HCs inactivated by >30%. Most mature (>P12) extrastriolar $K_V1.8^{-/-}$ type II HCs inactivated by <30% but some inactivated by >30% (7/30, 23%) because they had fast inactivation (B).

(**B**) Exemplar residual fast inactivation ($\tau_{FastInact}$ = 10 ms at +30 mV). For the 7 cells in this group, $\tau_{FastInact}$ = 30 ± 6 ms, amplitude of fast inactivation = 310 ± 70 pA; activation peak V_{half} = –15 ± 2 mV and slope factor = 12.4 ± 0.9 mV. These parameters are similar to g_A but for the much smaller conductance (one-way ANOVAs).

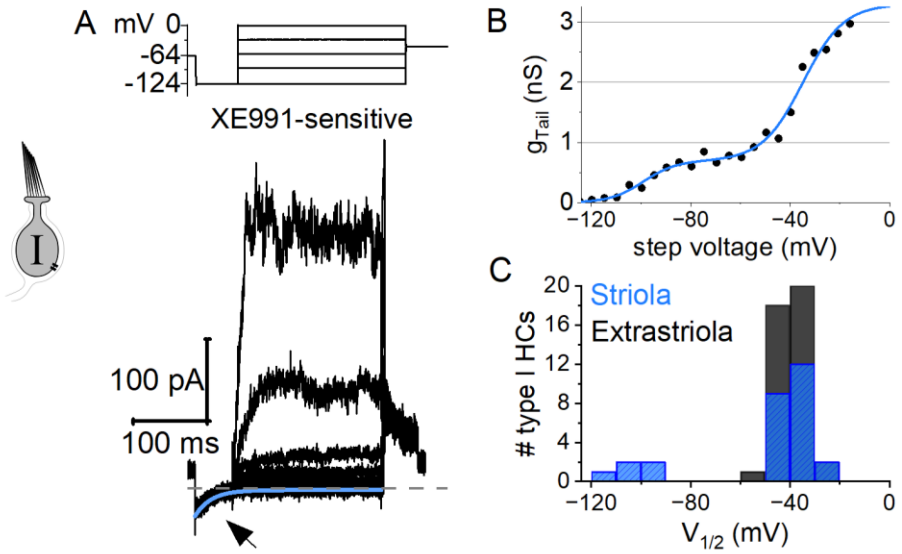

Supplemental Figure 5. A minority of striolar $K_V1.8^{-/-}$ type I HCs had a small low-voltage-activated outward rectifier current.

(**A**) Low-voltage-activated current from one cell was isolated by 10 µM XE991 (P39), suggesting it was a K_V7 current. Deactivation of XE991-sensitive current after step from –64 mV to –124 mV *(arrow*) was fit with exponential decay (τ = 21 ms).

(**B**) Tail G-V curve fit with a sum of two Boltzmann equations: $V_{half,1}$ = –102 ± 4 mV (n=5) and $V_{half,2}$ = –41 ± 1 mV. Ages: P11, 39, 202, 202, 202.

(**C**) Bimodal V_{half} distribution was specific to striolar type I HCs. 5/23 (22%; P6-P370) of striolar type I HCs had this low-voltage-activated component, but no extrastriolar type I HCs (0/45; P6-277).

794

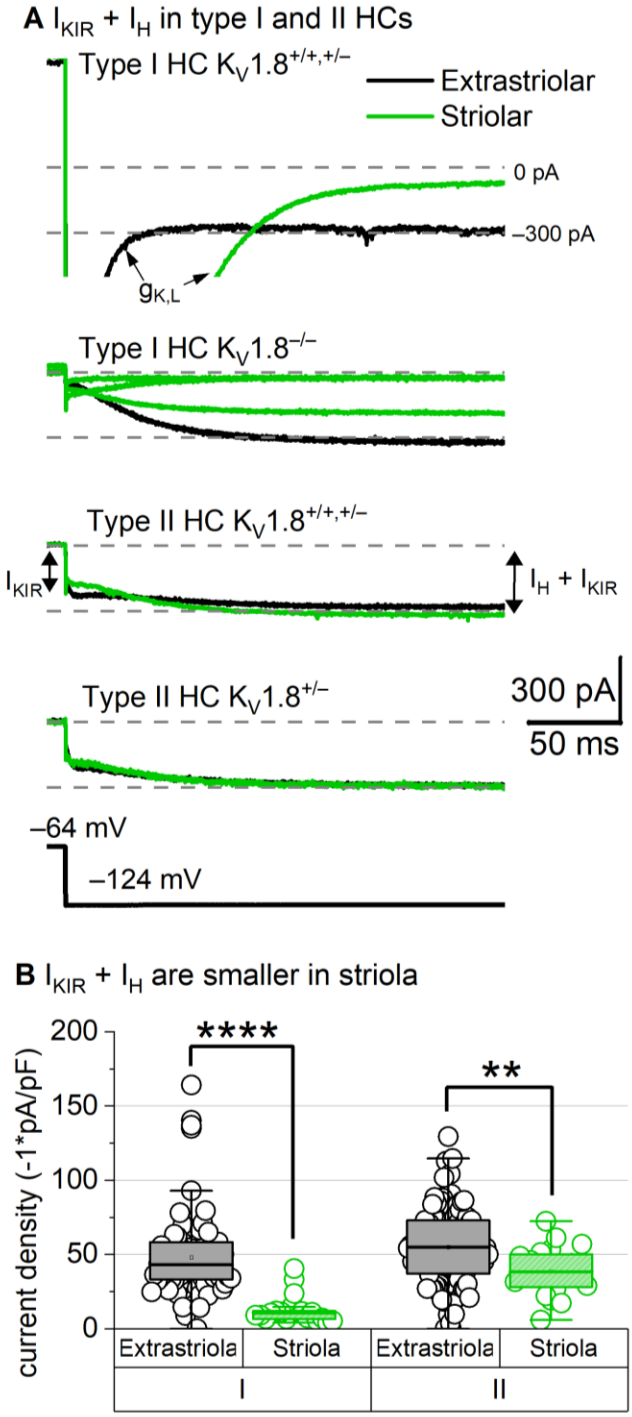

Supplemental Figure 6. No difference was detected in H (HCN) and KIR (fast inward rectifier) currents between $K_V1.8^{+/+}$ and $K_V1.8^{-/-}$ hair cells, consistent with a specific involvement of $K_V1.8$ in *Kcna10* expression.

(**A**) Hyperpolarizing voltage steps evoked I_{KIR} and I_{HCN} in $K_V1.8^{+/+,+/-,-/-}$ type I and II HCs. Note the prominent fast activation of I_{KIR} in type II but not type I HCs. Arrows in top panel show deactivation of $g_{K,L}$. I_H and I_{Kir} were measured as inward current after 250 ms at –124 mV.

(**B**) Summed I_{KIR} and I_H density was the same across genotypes but smaller in striola than extrastriola (see Supplemental Table 2 for statistics).

Supplemental Table 1. *Test of sex differences in hair cell K_V channel data.*

Cell Type	Parameter	Subgroup	Male vs Female posthoc p-value	Test
Type I HC	Tail V_{half}	+/+,+/– –/–	0.0023 ** [a] 0.57	Normal, homogeneous variance ANOVA: Genotype (2 levels), Sex (2 levels), Zone (2 levels), Genotype*Sex.
	Tail S	+/+,+/– –/–	0.98 0.58	ANOVA: Genotype (2 levels), Sex (2 levels), Zone (2 levels), Genotype*Sex. Normal, homogeneous variance
	Tail $g_{Density}$	+/+,+/– –/–	0.999 0.936	Normal, nonhomogeneous variance Welch ANOVA: Genotype*Sex
Type II HC	Peak V_{half}	+/+,+/– –/–	0.95 0.28	Normal, homogeneous variance ANOVA: Genotype (2 levels), Sex (2 levels), Zone (2 levels), Genotype*Sex.
	Peak S	+/+,+/– –/–	0.999 0.97	Normal, homogeneous variance ANOVA: Genotype (2 levels), Sex (2 levels), Zone (2 levels), Genotype*Sex.
	Peak $g_{Density}$	+/+,+/– –/–	0.64 0.43	Normal, nonhomogeneous variance Welch ANOVA: Genotype*Sex
	% inactivation at 30 mV	+/+,+/– –/–	0.98 0.82	Normal, homogeneous variance ANOVA: Genotype (2 levels), Sex (2 levels), Zone (2 levels), Genotype*Sex.

[a] g, 0.9. Male $K_V1.8^{+/+,+/-}$, –85 ± 1 mV (40) vs. Female $K_V1.8^{+/+,+/-}$, –79 ± 2 mV (12)

Supplemental Table 2. *Detected zonal but not genotype differences in hair cell I_{KIR} and I_H.*

Cell Type	Zone	I_H + I_{Kir} current density (-1*pA/pF)	$K_v1.8^{+/+,+/-}$ *vs* $K_v1.8^{-/-}$ p-value	ES *vs* Striola p-value	Test
Type I HC	ES Striola	48 ± 3 (78) 13.0 ± 2 (19)	0.3	4E-9 **** [a]	Non-normal, KWA
Type II HC	ES Striola	55 ± 2 (116) 39 ± 4 (20)	0.19 (0.25 power)	0.0058 ** [b]	Normal, homogeneous variance. 2-way ANOVA: Genotype (2 levels), Zone (2 levels)

[a] g 1.4
[b] g 0.6